

# $\Xi_b \rightarrow \Xi$ form factors from lattice QCD and Standard-Model predictions for $\Xi_b \rightarrow \Xi\mu^+\mu^-$ and $\Xi_b \rightarrow \Xi\gamma$ decays

Callum Farrell and Stefan Meinel

*Department of Physics, University of Arizona, Tucson, AZ 85721, USA*

(Dated: March 18, 2026)

We present the first lattice QCD determination of the  $\Xi_b \rightarrow \Xi$  vector, axial-vector, and tensor form factors, which are relevant for the theory of rare decays including  $\Xi_b \rightarrow \Xi\ell^+\ell^-$  and  $\Xi_b \rightarrow \Xi\gamma$ . The calculation is performed with 2+1 flavors of domain-wall fermions at three different lattice spacings and pion masses in the range from approximately 430 to 230 MeV. The bottom quark is implemented using an anisotropic clover action. Three-point functions with a wide range of source-sink separations and model averaging are used to extract the ground-state contributions. We fit the dependence of the form factors on the momentum transfer, the pion mass, and the lattice spacing using modified  $z$  expansions that account for subthreshold branch cuts, and apply dispersive bounds and asymptotic-behavior constraints to achieve controlled uncertainties in the full semileptonic kinematic region. Using our form factor results, we present Standard-Model predictions for the  $\Xi_b^- \rightarrow \Xi^-\gamma$  and  $\Xi_b^- \rightarrow \Xi^-\mu^+\mu^-$  branching fractions and two angular observables.

## I. INTRODUCTION

Rare decays of  $b$ -hadrons have long been a focus of theoretical and experimental scrutiny in the search for physics beyond the Standard Model. Their persistent study has uncovered a variety of tensions between theoretical predictions and experimental measurements, often collectively referred to as the  $B$  anomalies (see, e.g., Ref. [1]). Even though hints for lepton-flavor universality violation in  $b \rightarrow s\ell^+\ell^-$  decays have disappeared after new measurements [2, 3], tensions with Standard-Model predictions persist in the branching fractions of  $B \rightarrow K^{(*)}\mu^+\mu^-$  and  $B_s \rightarrow \phi\mu^+\mu^-$  and in angular observables in the  $B \rightarrow K^*\mu^+\mu^-$  transitions [4–24]. Recent global fits [1, 16, 25–29] favor a significant shift solely in the Wilson coefficient  $C_9$ . To help discriminate the source of this shift from new physics or yet underestimated Standard-Model processes [30–42] it is useful to study  $b \rightarrow s\ell\ell$  transitions in several distinct decay modes, including baryonic decay modes. Baryonic  $b \rightarrow s\ell^+\ell^-$  decays are sensitive to all possible Dirac structures in the effective Hamiltonian, and the possible polarization of the initial baryon, as well as parity-violating weak decays of final-state baryon, enable new types of angular observables [43–50]. In this sector, the focus has been primarily on the bottom baryon with the largest production fraction, the  $\Lambda_b$ . The  $\Lambda_b \rightarrow \Lambda\ell^+\ell^-$  local form factors have been studied with a variety of theoretical tools in Refs. [51–73], and with lattice QCD in Refs. [74, 75]. Experimental measurements of the branching fraction and angular observables of the  $\Lambda_b \rightarrow \Lambda(\rightarrow p\pi)\mu^+\mu^-$  transition [76–78] were used in combination with a lattice QCD calculation of the local form factors [75] to constrain Wilson coefficients in Refs. [46, 50]. Next-generation lattice calculations of the  $\Lambda_b \rightarrow \Lambda$  form factors are now in progress [79].

With analyses of the  $\Lambda_b$  transitions reaching a more advanced stage, it is sensible to extend this baryonic perspective to another set of  $b \rightarrow s\ell^+\ell^-$  observables from the  $SU(3)$  partner processes  $\Xi_b \rightarrow \Xi\ell^+\ell^-$ . Although the  $\Xi_b^{0,-}$  have relatively lower production fractions, there is already some experimental interest in rare decays of the  $\Xi_b^-$ . An LHCb analysis of the  $\Xi_b^- \rightarrow \Xi^-\mu^+\mu^-$  mode with the combined Run 1 and 2 datasets is in progress, motivated by the expectation of low mesonic backgrounds from a distinctive decay topology and good efficiency reconstructing the charged particle decay chain of the  $\Xi_b^-$  [80]. Blinded measurements of the ratio  $r_{BR} = \mathcal{B}(\Xi_b^- \rightarrow \Xi^-\mu^+\mu^-)/\mathcal{B}(\Xi_b^- \rightarrow \Xi^-J/\psi(\rightarrow\mu^+\mu^-))$  are discussed in Ref. [80]. This promising experimental outlook motivates new theoretical work.

The individual form factors that describe the  $\Xi_b \rightarrow \Xi\ell^+\ell^-$  transitions were first estimated in the large recoil (low  $q^2$ ) limit with light-cone sum rules in Ref. [81] (see also Refs. [82] and [83] for phenomenological applications). Furthermore, enabled by the LHCb measurements of  $d\mathcal{B}(\Lambda_b \rightarrow \Lambda\mu^+\mu^-)/dq^2$  [76, 77], the values of  $d\mathcal{B}(\Xi_b^- \rightarrow \Xi^-\mu^+\mu^-)/dq^2$  (and other related decays) were estimated by flavor  $SU(3)$  symmetry in Ref. [84]. Recently, the form factors were calculated again at low  $q^2$  within the “pQCD framework” in Ref. [85], leading to new Standard-Model predictions of the  $\Xi_b \rightarrow \Xi\ell^+\ell^-$  differential branching fraction and angular observables. The predictions at high  $q^2$  depend on extrapolations of the form factors and have large uncertainty. A lattice QCD calculation of the form factors will be most precise at high  $q^2$  and is crucial for obtaining reliable Standard-Model predictions for the  $\Xi_b \rightarrow \Xi\ell^+\ell^-$  differential branching fraction and angular observables.

It is also interesting to study the radiative decays  $\Xi_b \rightarrow \Xi\gamma$ , whose rates depend on the tensor form factors at  $q^2 = 0$ . Like its better studied counterpart  $\Lambda_b \rightarrow \Lambda\gamma$ , which was first observed by LHCb in 2019 [86], these processes are sensitive to the helicity structure of the  $b \rightarrow s\gamma$  transition [43, 44], can be used to search for possible new sources of  $CP$  violation [44], and constrain the Wilson coefficients  $C_7$  and  $C_7'$ . A 2021 LHCb search [87] set an upper limit for the  $\Xi_b \rightarrow \Xi\gamma$  branching fraction. The Standard-Model predictions of Refs. [88–92] are below this limit, while

the prediction of Ref. [93] is above. A lattice calculation of the relevant  $\Xi_b \rightarrow \Xi$  tensor form factors can clarify this situation.

In this work, we present the first lattice QCD calculation of the vector, axial-vector and tensor form factors governing the  $\Xi_b \rightarrow \Xi \ell^+ \ell^-$  and  $\Xi_b \rightarrow \Xi \gamma$  transitions, using domain-wall fermions for the light and strange quarks and an anisotropic clover action for the bottom quark. On four ensembles, with lattice spacings ranging from 0.073 to 0.111 fm and pion masses ranging from 0.232 to 0.431 GeV, we compute three-point functions for 15 unique source-sink separations to reliably extract the ground-state form factors. We then perform chiral-continuum-kinematic extrapolations using modified  $z$  expansions, with constraints from both dispersive bounds and form factor asymptotics to achieve controlled uncertainties in the full semileptonic kinematic region. Using our form factor results, we obtain Standard-Model predictions for the  $\Xi_b^- \rightarrow \Xi^- \gamma$  and  $\Xi_b^- \rightarrow \Xi^- \mu^+ \mu^-$  branching fractions and two angular observables.

## II. FORM-FACTOR DEFINITIONS

As in our recent calculation Ref. [94], and as in the previous calculations of Refs. [75, 95–97], we define the form factors in the helicity-based scheme first described in Ref. [62]. In this scheme, the hadronic matrix elements are written as

$$\begin{aligned} \langle \Xi(p', s') | \bar{s} \gamma^\mu c | \Xi_b(p, s) \rangle &= \bar{u}_\Xi(p', s') \left[ f_0(q^2) (m_{\Xi_b} - m_\Xi) \frac{q^\mu}{q^2} \right. \\ &\quad + f_+(q^2) \frac{m_{\Xi_b} + m_\Xi}{s_+} \left( p^\mu + p'^\mu - (m_{\Xi_b}^2 - m_\Xi^2) \frac{q^\mu}{q^2} \right) \\ &\quad \left. + f_\perp(q^2) \left( \gamma^\mu - \frac{2m_\Xi}{s_+} p^\mu - \frac{2m_{\Xi_b}}{s_+} p'^\mu \right) \right] u_{\Xi_b}(p, s), \end{aligned} \quad (1)$$

$$\begin{aligned} \langle \Xi(p', s') | \bar{s} \gamma^\mu \gamma_5 c | \Xi_b(p, s) \rangle &= -\bar{u}_\Xi(p', s') \gamma_5 \left[ g_0(q^2) (m_{\Xi_b} + m_\Xi) \frac{q^\mu}{q^2} \right. \\ &\quad + g_+(q^2) \frac{m_{\Xi_b} - m_\Xi}{s_-} \left( p^\mu + p'^\mu - (m_{\Xi_b}^2 - m_\Xi^2) \frac{q^\mu}{q^2} \right) \\ &\quad \left. + g_\perp(q^2) \left( \gamma^\mu + \frac{2m_\Xi}{s_-} p^\mu - \frac{2m_{\Xi_b}}{s_-} p'^\mu \right) \right] u_{\Xi_b}(p, s), \end{aligned} \quad (2)$$

$$\begin{aligned} \langle \Xi(p', s') | \bar{s} i \sigma^{\mu\nu} q_\nu b | \Xi_b(p, s) \rangle &= -\bar{u}_\Xi(p', s') \left[ h_+(q^2) \frac{q^2}{s_+} \left( p^\mu + p'^\mu - (m_{\Xi_b}^2 - m_\Xi^2) \frac{q^\mu}{q^2} \right) \right. \\ &\quad \left. + h_\perp(q^2) (m_{\Xi_b} + m_\Xi) \left( \gamma^\mu - \frac{2m_\Xi}{s_+} p^\mu - \frac{2m_{\Xi_b}}{s_+} p'^\mu \right) \right] u_{\Xi_b}(p, s), \end{aligned} \quad (3)$$

$$\begin{aligned} \langle \Xi(p', s') | \bar{s} i \sigma^{\mu\nu} q_\nu \gamma_5 b | \Xi_b(p, s) \rangle &= -\bar{u}_\Xi(p', s') \gamma_5 \left[ \tilde{h}_+(q^2) \frac{q^2}{s_-} \left( p^\mu + p'^\mu - (m_{\Xi_b}^2 - m_\Xi^2) \frac{q^\mu}{q^2} \right) \right. \\ &\quad \left. + \tilde{h}_\perp(q^2) (m_{\Xi_b} - m_\Xi) \left( \gamma^\mu + \frac{2m_\Xi}{s_-} p^\mu - \frac{2m_{\Xi_b}}{s_-} p'^\mu \right) \right] u_{\Xi_b}(p, s), \end{aligned} \quad (4)$$

with  $q = p - p'$ ,  $s_\pm = (m_{\Xi_b} \pm m_\Xi)^2 - q^2$ , and  $\sigma^{\mu\nu} = \frac{i}{2}(\gamma^\mu \gamma^\nu - \gamma^\nu \gamma^\mu)$ . The helicity form factors satisfy the endpoint relations

$$f_0(0) = f_+(0), \quad (5)$$

$$g_0(0) = g_+(0), \quad (6)$$

$$h_\perp(0) = \tilde{h}_\perp(0) \quad (7)$$

$$g_\perp(q_{\max}^2) = g_+(q_{\max}^2), \quad (8)$$

$$\tilde{h}_\perp(q_{\max}^2) = \tilde{h}_+(q_{\max}^2), \quad (9)$$

with  $q_{\max}^2 = (m_{\Xi_b} - m_\Xi)^2$ .

Label	$N_s^3 \times N_t \times N_5$	$\beta$	$a$ [fm]	$2\pi/L$ [GeV]	$am_{u,d}$	$m_\pi$ [GeV]	$am_s^{(\text{sea})}$	$am_s^{(\text{val})}$	$am_Q^{(b)}$	$\nu^{(b)}$	$c_{E,B}^{(b)}$	$N_{\text{ex}}$	$N_{\text{sl}}$
C01	$24^3 \times 64 \times 16$	2.13	0.1106(3)	0.4673(13)	0.01	0.4312(13)	0.04	0.0323	7.3258	3.1918	4.9625	283	2264
C005	$24^3 \times 64 \times 16$	2.13	0.1106(3)	0.4673(13)	0.005	0.3400(11)	0.04	0.0323	7.3258	3.1918	4.9625	311	2488
F004	$32^3 \times 64 \times 16$	2.25	0.0828(3)	0.4680(17)	0.004	0.3030(12)	0.03	0.0248	3.2823	2.0600	2.7960	251	2008
F1M	$48^3 \times 96 \times 12$	2.31	0.0728(3)	0.3545(13)	0.002144	0.2320(10)	0.02144	0.02217	2.3867	1.8323	2.4262	113	1808

TABLE I. Lattice and action parameters for each the of ensembles. The ensemble generation and lattice spacings are discussed in Refs. [98–100]. The light valence quarks are implemented with the same action as the sea quarks, with masses set equal to the sea quark values. The strange valence quarks are also implemented with the same action, but with masses tuned to the physical point. The F1M ensemble uses a Möbius domain-wall action [100], while C01, C005, and F004 use a Shamir domain-wall action [98, 99]. The bottom quark mass  $am_Q^{(b)}$ , the anisotropy parameter  $\nu^{(b)}$ , and the chromoelectric/chromomagnetic clover coefficients  $c_E^{(b)} = c_B^{(b)}$  values and tunings are discussed in Ref. [79].  $N_{\text{ex}}$  and  $N_{\text{sl}}$  are the number of exact and sloppy (computed with reduced conjugate-gradient iteration counts) samples used in the all-mode-averaging procedure [101, 102].

### III. LATTICE CALCULATION AND CORRELATION-FUNCTION FITS

This calculation was performed with the same set of ensembles and actions as in our recent work [94]. For the light quarks, we use the 2+1 flavor domain-wall fermion, Iwaski gauge action ensembles generated by the RBC and UKQCD collaborations [98–100], while for the heavy quark we again use an anisotropic clover action analogous to Ref. [103]. The parameters  $am_Q^{(b)}$ ,  $\nu^{(b)}$ , and  $c_E^{(b)} = c_B^{(b)}$  of the latter are tuned nonperturbatively to give the experimental values of the  $B_s$  meson rest mass, kinetic mass, and hyperfine splitting. The tuning procedure is detailed in Ref [79] (for the bare parameters we use the notation of Ref. [104], whereas Ref. [103] uses  $m_0 = m_Q$ ,  $\zeta = \nu$ ,  $c_P = c_E = c_B$ ). The major lattice and action parameters for each of the four ensembles are listed in Table I.

For the  $\Xi_b$  and  $\Xi$  baryons, we use the interpolating fields

$$\Xi_{b\alpha} = \epsilon_{abc}(C\gamma_5)_{\beta\gamma}d_\beta^a s_\gamma^b b_\alpha^c, \quad \Xi_\alpha = \epsilon_{abc}(C\gamma_5)_{\beta\gamma}d_\beta^a s_\gamma^b s_\alpha^c. \quad (10)$$

The smearing parameters for the quark fields are listed in Table II. We compute the forward and backward two-point correlation functions

$$\begin{aligned} C_{\delta\alpha}^{(2,\Xi,\text{fw})}(\mathbf{p}', t) &= \sum_{\mathbf{y}} e^{-i\mathbf{p}'\cdot(\mathbf{y}-\mathbf{x})} \langle \Xi_\delta(x_0 + t, \mathbf{y}) \bar{\Xi}_\alpha(x_0, \mathbf{x}) \rangle, \\ C_{\delta\alpha}^{(2,\Xi,\text{bw})}(\mathbf{p}', t) &= \sum_{\mathbf{y}} e^{-i\mathbf{p}'\cdot(\mathbf{x}-\mathbf{y})} \langle \Xi_\delta(x_0, \mathbf{x}) \bar{\Xi}_\alpha(x_0 - t, \mathbf{y}) \rangle, \\ C_{\delta\alpha}^{(2,\Xi_b,\text{fw})}(t) &= \sum_{\mathbf{y}} \langle \Xi_{b\delta}(x_0 + t, \mathbf{y}) \bar{\Xi}_{b\alpha}(x_0, \mathbf{x}) \rangle, \\ C_{\delta\alpha}^{(2,\Xi_b,\text{bw})}(t) &= \sum_{\mathbf{y}} \langle \Xi_{b\delta}(x_0, \mathbf{x}) \bar{\Xi}_{b\alpha}(x_0 - t, \mathbf{y}) \rangle, \end{aligned} \quad (11)$$

and the forward and backward three-point correlation functions

$$\begin{aligned} C_{\delta\alpha}^{(3,\text{fw})}(\Gamma, \mathbf{p}', t, t') &= \sum_{\mathbf{y}, \mathbf{z}} e^{-i\mathbf{p}'\cdot(\mathbf{x}-\mathbf{y})} \langle \Xi_\delta(x_0, \mathbf{x}) J_\Gamma(x_0 - t + t', \mathbf{y}) \bar{\Xi}_{b\alpha}(x_0 - t, \mathbf{z}) \rangle, \\ C_{\delta\alpha}^{(3,\text{bw})}(\Gamma, \mathbf{p}', t, t') &= \sum_{\mathbf{y}, \mathbf{z}} e^{-i\mathbf{p}'\cdot(\mathbf{y}-\mathbf{x})} \langle \Xi_{b\delta}(x_0 + t, \mathbf{z}) J_\Gamma^\dagger(x_0 + t', \mathbf{y}) \bar{\Xi}_\alpha(x_0, \mathbf{x}) \rangle, \end{aligned} \quad (12)$$

where  $J_\Gamma$  is discussed in Eq. (13) below. We take our initial state  $\Xi_b$  to have zero spatial momentum and use sequential propagators for the bottom quark in the three-point correlation functions. The correlation functions are computed with light and strange quark propagators with source position  $(x_0, \mathbf{x})$ , which are reused from Ref. [105] for C01, C005, F004 and from Ref. [79] for F1M.

The  $b \rightarrow s$  currents  $J_\Gamma$  are structured as

$$J_\Gamma = \rho_\Gamma \sqrt{Z_V^{\text{ll}} Z_V^{\text{bb}}} \left[ \bar{s} \Gamma b + \mathcal{O}(a)\text{-improvement terms} \right], \quad (13)$$

with the complete forms of the vector and axial vector currents with the  $\mathcal{O}(a)$ -improvement terms are given in Eqs. (18)-(21) of Ref. [95], while the tensor current is given explicitly in Eq. (24) of Ref. [75]. We again use the

Ensemble	Up and down quarks		Strange quarks		Bottom quarks	
	$N_{\text{Gauss}}$	$\sigma_{\text{Gauss}}/a$	$N_{\text{Gauss}}$	$\sigma_{\text{Gauss}}/a$	$N_{\text{Gauss}}$	$\sigma_{\text{Gauss}}/a$
C005, C01	30	4.350	30	4.350	10	2.0
F004	60	5.728	60	5.728	16	2.667
F1M	130	8.9	70	6.6	20	3.0

TABLE II. Parameters for the smearing of the quark fields in the baryon interpolating fields. The Gaussian smearing is defined as in Eq. (8) of Ref. [106]. For the up, down, and strange quarks, we used APE-smearred gauge links [107] with  $N_{\text{APE}} = 25$  and  $\alpha_{\text{APE}} = 2.5$  in the Gaussian smearing kernel. For the bottom quarks, we use Stout-smearred [108] gauge links with  $N_{\text{Stout}} = 10$  and  $\rho_{\text{Stout}} = 0.08$  in the Gaussian smearing.

Ensemble	$Z_V^{(ll)}$	$Z_V^{(bb)}$
C005, C01	0.71273(26) [99]	9.0631(84) [79]
F004	0.7440(18) [99]	4.7449(21) [79]
F1M	0.7639(42) [111]	3.7777(23) [79]

TABLE III. Nonperturbative results for the renormalization factors of the temporal components of the flavor-conserving vector currents.

mostly nonperturbative renormalization scheme [109, 110], in which most of the renormalization is captured in the renormalization factors of the temporal parts of the light-to-light vector current ( $Z_V^{ll}$ ) and bottom-to-bottom vector current ( $Z_V^{bb}$ ), which are determined nonperturbatively using charge conservation. The values of these factors for each ensemble are given in Table III.

Table IV lists both the residual matching factors  $\rho_\Gamma$  and the  $\mathcal{O}(a)$ -improvement coefficients for the vector and axial vector currents. For the tensor currents, one-loop results for these coefficients were not available, and we used the mean-field improved tree-level values as in Ref. [75], with the values of  $d_1$  also given in Table IV. This contributes an additional source of systematic uncertainty, which is discussed in detail in Section IV.

As in Refs. [75, 94–97], we compute the helicity form factors from ratios of three-point and two-point correlation functions that are designed to cancel the overlap factors and time dependence of the ground-state contribution. For

Parameter	C005, C01	F004	F1M
$\rho_{V^0} = \rho_{A^0}$	1.027(10)	1.0166(51)	1.0112(74)
$\rho_{V^j} = \rho_{A^j}$	0.9972(11)	0.9940(18)	0.9922(25)
$c_{V^0}^R = c_{A^0}^R$	0.0558(73)	0.0547(57)	0.0541(58)
$c_{V^0}^L = c_{A^0}^L$	-0.0099(39)	-0.0095(29)	-0.0093(29)
$c_{V^j}^R = c_{A^j}^R$	0.0485(45)	0.0480(37)	0.0477(37)
$c_{V^j}^L = c_{A^j}^L$	-0.0033(13)	-0.00200(61)	-0.00129(93)
$d_{V^j}^R = -d_{A^j}^R$	-0.00079(31)	-0.00120(37)	-0.00142(43)
$d_{V^j}^L = -d_{A^j}^L$	0.00180(70)	0.00047(14)	-0.00026(74)
$d_1$	0.07403	0.07182	0.06797

TABLE IV. Perturbative renormalization and  $\mathcal{O}(a)$ -improvement coefficients for the  $b \rightarrow s$  currents used in Eq. (13). For the C005/C01 and F004 ensembles, they were computed by C. Lehner at one loop in mean-field-improved lattice perturbation theory [112]. For these two ensembles, the uncertainties given in Table IV correspond to the change in the central value when changing the strong coupling from a mean-field lattice  $\overline{\text{MS}}$  coupling  $\alpha_{s,\text{lat}}^{\overline{\text{MS}}}(a^{-1})$  to the continuum  $\overline{\text{MS}}$  coupling  $\alpha_{s,\text{ctm}}^{\overline{\text{MS}}}(a^{-1})$  [113]. For the newer F1M ensemble, perturbative results were not available, and therefore we estimated the coefficients through an extrapolation of the values from the C005/C01 and F004 ensembles, done linearly in the lattice spacing. In this case, the uncertainties given in the table are the sum (in quadrature) of the F004 uncertainties and the shifts in the central values between F004 and F1M.

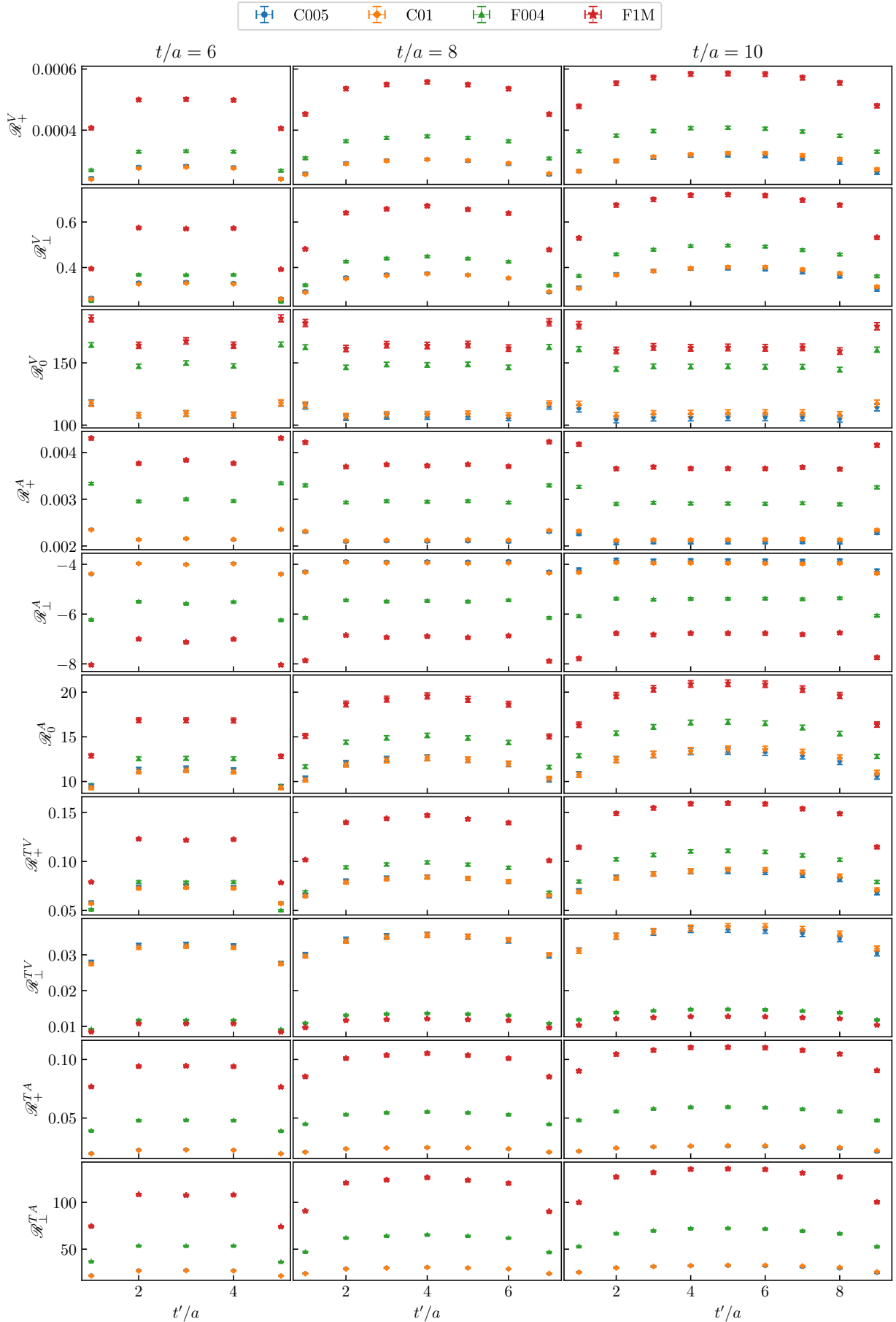


FIG. 1. The  $t'$  dependence of the different ratios with vector, axial vector and tensor current insertions for three different values of the source-sink separation,  $t$ . The data from the C005, C01, and F004 ensembles are shown at  $|\mathbf{p}'|^2 = 1 \cdot (\frac{2\pi}{L})^2$ , and the data from the F1M ensemble are shown at  $|\mathbf{p}'|^2 = 2 \cdot (\frac{2\pi}{L})^2$ . The plots are in units of  $\text{GeV}^{-2}$  for the dimensional ratios ( $\mathcal{R}_\perp^V, \mathcal{R}_0^V, \mathcal{R}_\perp^A, \mathcal{R}_0^A, \mathcal{R}_+^{TV}, \mathcal{R}_+^{TA}$ ) and of  $\text{GeV}^{-4}$  for ( $\mathcal{R}_\perp^{TV}, \mathcal{R}_\perp^{TA}$ ); the uncertainty from the lattice spacing is not shown.

Ensemble	$am_{\Xi_b}$	$am_{\Xi}$	$am_B$	$am_K$
C01	3.2956(33)	0.8078(23)	2.9792(19)	0.32457(45)
C005	3.2718(38)	0.7821(22)	2.9729(20)	0.30706(54)
F004	2.4447(42)	0.5832(14)	2.2248(10)	0.22492(58)
F1M	2.1485(27)	0.5011(12)	1.9545(13)	0.19073(19)

TABLE V. Hadron masses in lattice units. The  $B$  and  $K$  masses are used in the chiral-continuum-kinematic extrapolations of the form factors.

example, the  $h_+$  form factor is obtained from the ratio

$$\mathcal{R}_+^{TV}(\mathbf{p}', t, t') = \frac{r_\mu[(1, \mathbf{0})] r_\nu[(1, \mathbf{0})] \text{Tr} \left[ C^{(3, \text{fw})}(\mathbf{p}', i\sigma^{\mu\rho} q_\rho, t, t') C^{(3, \text{bw})}(\mathbf{p}', i\sigma^{\nu\lambda} q_\lambda, t, t-t') \right]}{\text{Tr} \left[ C^{(2, \Xi, \text{av})}(\mathbf{p}', t) \right] \text{Tr} \left[ C^{(2, \Xi_b, \text{av})}(t) \right]}, \quad (14)$$

where we use the averages of the forward and backward two-point functions, and where  $r_\mu[(1, \mathbf{0})]$  is a polarization vector that projects to the desired helicity, defined as

$$r[n] = n - \frac{(q \cdot n)}{q^2} q. \quad (15)$$

The dependence on the current insertion time  $t'$  of  $\mathcal{R}_+^{TV}$  and the other ratios is shown in Fig. 1. From these ratios we construct new quantities such as, in the case of the form factor  $h_+$ ,

$$R_{h_+}(|\mathbf{p}'|, t) = \frac{2}{E_\Xi - m_\Xi} \sqrt{\frac{E_\Xi}{(E_\Xi + m_\Xi)}} \mathcal{R}_+^{TV}(|\mathbf{p}'|, t, t/2), \quad (16)$$

which, because the excited-state contamination is suppressed at large Euclidean time, asymptotically approach the value of the form factor. We average over the directions of  $\mathbf{p}'$ , while the  $t'$  dependence is removed by evaluating the ratio at  $t' = t/2$  (or averaging over the two mid-points for odd  $t/a$ ). The values of  $m_{\Xi_b}$  and  $m_\Xi$  on each ensemble are given in Table V. The quantities  $R_{f_+}$ ,  $R_{f_\perp}$ ,  $R_{f_0}$ ,  $R_{g_+}$ ,  $R_{g_\perp}$ , and  $R_{g_0}$  are given explicitly in Eqs. (46)-(60) of Ref. [95], while  $R_{h_+}$ ,  $R_{h_\perp}$ ,  $R_{\tilde{h}_+}$ , and  $R_{\tilde{h}_\perp}$  are given in Eqs. (27)-(30) of Ref. [75]. These were computed at source-sink separations of  $t/a = 4, 5, \dots, 15$  on the C01 and C005 ensembles,  $t/a = 5, 6, \dots, 15$  on F004 and  $t/a = 6, 7, \dots, 20$  on F1M. We computed the ratios for values of  $\Xi$  spatial momenta squared of  $\{1, 2, 3, 4, 5, 6, 8, 9, 10\} \cdot (\frac{2\pi}{L})^2$  on C005, C01, F004 and  $\{1, 2, 3, 4, 5, 6, 8, 9, 10, 11, 12, 13, 14, 16\} \cdot (\frac{2\pi}{L})^2$  on F1M.

To extrapolate the functions  $R_f$  to infinite source-sink separation, we use the same fit functions (for each form factor  $f$ , each value of  $n = |\mathbf{p}'|^2/(2\pi/L)^2$ , and each ensemble  $i$ ) as in our previous calculations [75, 94–97]:

$$R_{f,i,n}(t) = f_{i,n} + A_{f,i,n} e^{-\delta E_{f,i,n} t}, \quad \delta E_{f,i,n} = \delta E_{\min} + e^{l_{f,i,n}} \text{ GeV}, \quad (17)$$

parameterized by  $f_{i,n}$ ,  $A_{f,i,n}$ , and  $l_{f,i,n}$ . The dominant excited-state contamination is captured in the exponential term, while  $f_{i,n}$  is the ground-state value of the form factor. As we did in Ref. [94], we set the minimum energy gap  $\delta E_{\min}$  to 100 MeV. To ensure the energy gap parameters  $l_{f,i,n}$  do not widely vary between the different ensembles with the same value of  $L$ , they are again constrained by priors, as in Eq. (70) of Ref. [95]. For some data points at higher momenta where the quantities  $R_{f,i,n}$  had larger error bars and did not display any curvature, the exponential term was omitted from the fit function.

As previously in Ref. [75, 94–97], the data for the three vector form factors ( $f = f_+, f_\perp, f_0$ ), the three axial-vector form factors ( $f = g_+, g_\perp, g_0$ ), as well as ( $f = h_+, h_\perp$ ) and ( $f = \tilde{h}_+, \tilde{h}_\perp$ ), are fitted simultaneously for a given momentum index  $n$ . These fits again also include data in the Weinberg basis to stabilize the extrapolations.

We estimate the systematic uncertainties from these fits with the same “perfect model” Akaike information criterion (AIC) Refs. [114, 115] that we utilized in our recent work on  $\Xi_c \rightarrow \Xi$  [94]. As described in Refs. [114, 115], the AIC average for a fit parameter is a weighted average with the weights determined by an information criterion (in this case the “perfect model” AIC). The variance of the AIC average, computed using Eq. (24) of Ref. [94], includes the systematic uncertainty resulting from the choice of fit ranges. We follow a similar prescription as in Ref. [94], and randomly sample the high-dimensional space of  $t_{\min}$ ’s for each simultaneous fit. For every individual form factor, we draw each  $t_{\min}$  from a uniform random distribution ranging from a value equal to or near the smallest value for which we have data, to a value that is larger by some chosen  $\delta$  (so  $\delta$  corresponds to the width of the random distribution

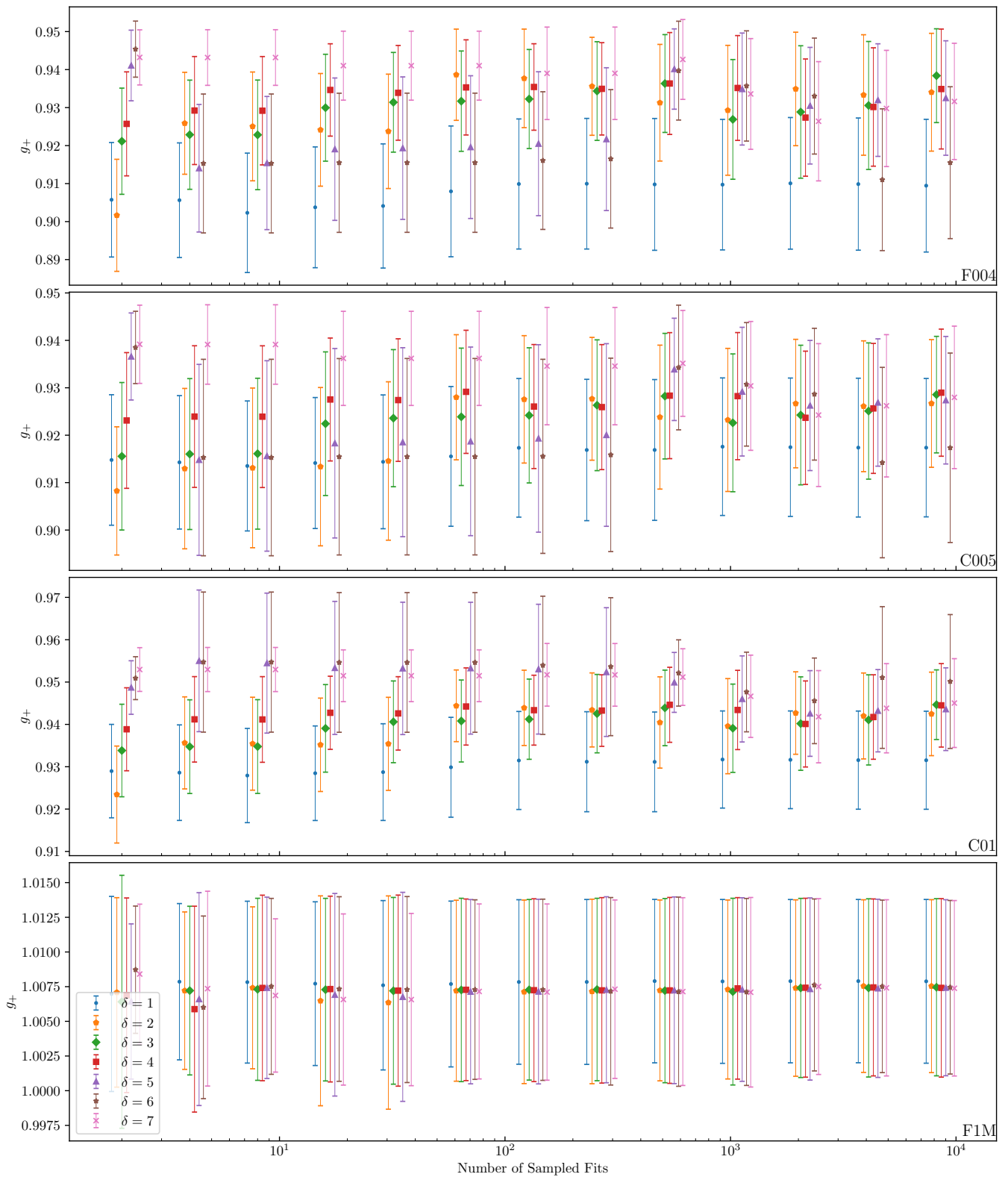


FIG. 2. Evolution of the AIC average and uncertainty of the form factor  $g_+$  at  $|\mathbf{p}'|^2 = 1 \cdot (\frac{2\pi}{L})^2$  as a function of the number of sample fits, for widths of the  $t_{\min}$  random distributions equal to  $\delta = 1, \dots, 7$  (in lattice units). As in Ref. [94], we found that values of  $\delta > 4$  could require larger numbers of sample fits for the AIC average to converge, but still tended toward consistent central values. As before, we use  $\delta = 4$  and  $\mathcal{O}(10,000)$  sample fits to obtain the final estimates.

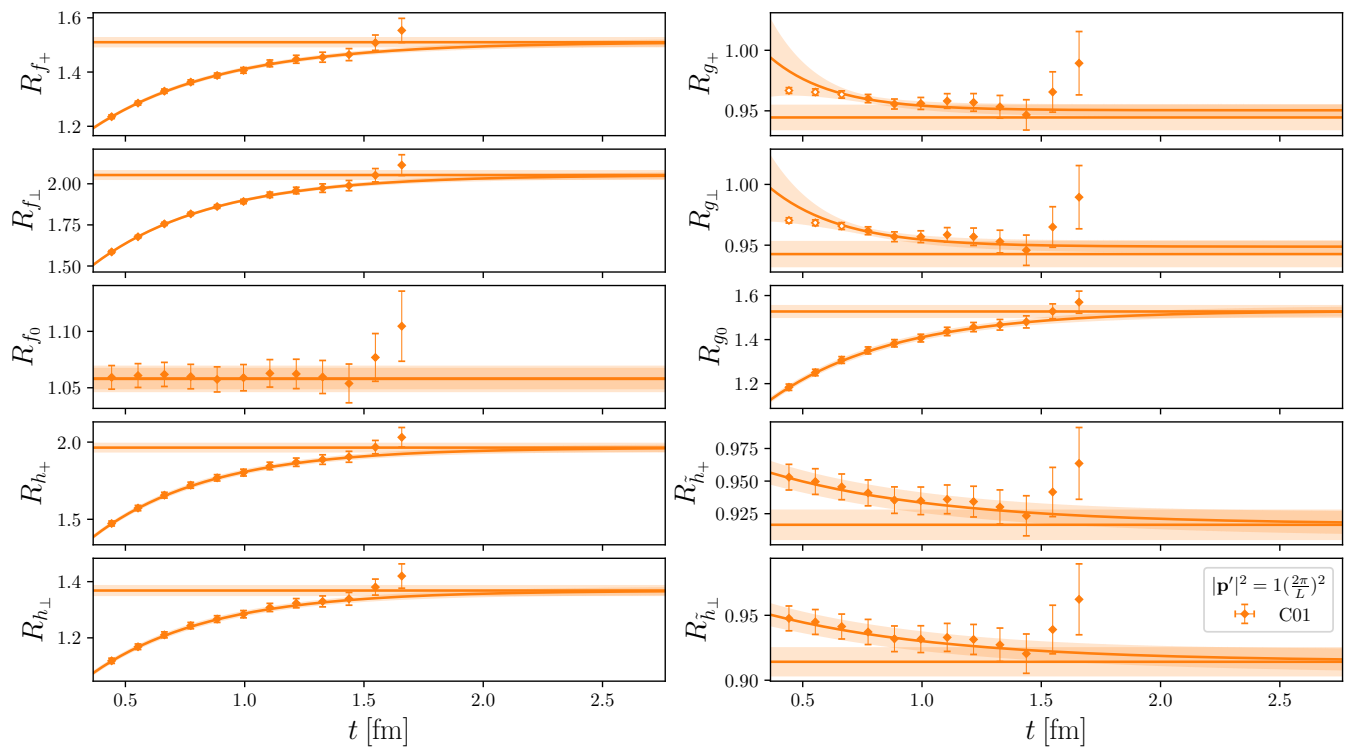


FIG. 3. AIC fit results for  $R_f(|\mathbf{p}'|, t)$  on the C01 ensemble at  $|\mathbf{p}'|^2 = 1(2\pi/L)^2$ . The curves going through the data points belong to the sample fit with the highest model weight, with the bands showing only the statistical uncertainty, whereas the horizontal bands depict to the AIC average values of the extracted ground-state form factors and their total uncertainty. Data points plotted with open symbols were omitted in the highest-model-weight fit.

of  $t_{\min}$ ). Performing a large enough number of these fits with randomly selected  $t_{\min}$ 's allows us to estimate the AIC average. We again investigated the dependence of the AIC average estimate on the choice of  $\delta$  and the number of sampled fits, which are shown for an example form factor in Fig. 2. As in Ref. [94], the final estimates were obtained with  $\delta = 4$  and  $\mathcal{O}(10,000)$  fits. We again found consistent AIC average values for  $\delta \geq 2$  and ( $\geq 7,000$ ) random fits. As in Ref [94], for some of the AIC extrapolated values at high values of  $q^2$ , the term that captures the systematic error in the AIC average [Eq. (24) of Ref. [94]], was often far smaller than at low values of  $q^2$ . Therefore, to be more conservative, for all form factors on all ensembles, we computed the average of that term across the entire  $q^2$  range and replaced any value that fell below it by the average value.

Sample results of this fit procedure are shown in Fig. 3 for the ensemble C01 at  $|\mathbf{p}'|^2 = 1 \cdot (\frac{2\pi}{L})^2$ . Both the AIC average value (and uncertainty) and the results of the highest-weight fit are shown for each of the form factors, while example fits for the other ensembles are shown in Fig. 9 in the Appendix.

#### IV. CHIRAL-CONTINUUM-KINEMATIC EXTRAPOLATIONS

We use BGL-type series expansions [116–118] to parametrize the  $q^2$  dependence of the form factors in the physical limit ( $a = 0$ ,  $m_\pi = m_{\pi, \text{phys}}$ ). We define

$$z(q^2, t_0, t_+) = \frac{\sqrt{t_+ - q^2} - \sqrt{t_+ - t_0}}{\sqrt{t_+ - q^2} + \sqrt{t_+ - t_0}}. \quad (18)$$

This transformation maps the complex  $q^2$  plane onto the unit disk, with the parameter  $t_0$  defining which particular value of  $q^2$  is mapped to  $z = 0$ ; we use

$$t_0 = q_{\max}^2 = (m_{\Xi_b} - m_\Xi)^2. \quad (19)$$

The parameters  $t_+$  are set to the positions at which the two-particle branch cuts along the real  $q^2$  axis begin, which is different for the different form factors. Since our calculation is performed in the limit of exact isospin symmetry,

we have

$$\begin{aligned} t_{+}^{f_{+}, f_{\perp}, f_0, h_{+}, h_{\perp}} &= (m_B + m_K)^2, \\ t_{+}^{g_{+}, g_{\perp}, g_0, \tilde{h}_{+}, \tilde{h}_{\perp}} &= (m_{B^*} + m_K)^2. \end{aligned} \quad (20)$$

We fit the lattice data with the functions

$$\begin{aligned} f(q^2) &= \frac{1}{\mathcal{P}_f(q^2)\phi_f(q^2)} \left[ a_0^f \left( 1 + c_0^f \frac{m_{\pi}^2 - m_{\pi, \text{phys}}^2}{\Lambda_{\chi}^2} + \tilde{c}_0^f \frac{m_{\pi}^3 - m_{\pi, \text{phys}}^3}{\Lambda_{\chi}^3} \right) \right. \\ &\quad \left. + a_1^f \left( 1 + c_1^f \frac{m_{\pi}^2 - m_{\pi, \text{phys}}^2}{\Lambda_{\chi}^2} \right) z(q^2, q_{\text{max}}^2, t_{+}^f) + \sum_{n=2}^{N+M} a_n^f [z(q^2, q_{\text{max}}^2, t_{+}^f)]^n \right] \\ &\quad \times \left[ 1 + b^f a^2 |\mathbf{p}'|^2 + d^f a^2 \Lambda_{\text{had}}^2 + \tilde{b}^f a^4 |\mathbf{p}'|^4 + \tilde{d}^f a^3 \Lambda_{\text{had}}^3 + \tilde{d}^f a^4 \Lambda_{\text{had}}^4 + j^f a^4 |\mathbf{p}'|^2 \Lambda_{\text{had}}^2 \right], \end{aligned} \quad (21)$$

which in the physical limit ( $a = 0$ ,  $m_{\pi} = m_{\pi, \text{phys}}$ ) simplify to the form

$$f(q^2) = \frac{1}{\mathcal{P}_f(q^2)\phi_f(q^2)} \sum_{n=0}^{N+M} a_n^f [z(q^2, q_{\text{max}}^2, t_{+}^f)]^n. \quad (22)$$

Here, the functions  $\mathcal{P}_f(q^2)$  are the Blaschke factors

$$\mathcal{P}_f(q^2) = z(q^2, [m_{\text{pole}}^f]^2, t_{+}^f), \quad (23)$$

with the pole masses listed in Table VI. The functions  $\phi_f(q^2)$  are the *outer functions*, which were constructed in Ref. [117] and are given in Appendix B. The scale factors  $\Lambda_{\text{had}} = 300$  MeV and  $\Lambda_{\chi} = 4\pi f_{\pi}$  (with  $f_{\pi} = 132$  MeV) allow all parameters to remain dimensionless. When doing the fit using Eq. (21), we use the lattice hadron masses from each individual data set<sup>1</sup>, to evaluate  $z(q^2, q_{\text{max}}^2, t_{+}^f)$  and the outer functions, but we use the physical hadron masses from experiment [119],  $m_{\Xi_b^-} = 5.797$  GeV,  $m_{\Xi_b^0} = 1.3217$  GeV,  $m_B = 5.279$  GeV,  $m_{B^*} = 5.324$  GeV,  $m_K = 0.494$  GeV, to evaluate the Blaschke factors. When evaluating the physical-limit form factors using Eq. (22), we use the physical hadron masses throughout.

In our fit using Eq. (21), we implement the endpoint constraints (8) and (9), which apply to the point  $z = 0$ , by eliminating  $a_0^{g_{\perp}}$  and  $a_0^{\tilde{h}_{\perp}}$  through

$$a_0^{g_{\perp}} = \frac{\phi_{g_{\perp}}(t_0)}{\phi_{g_{+}}(t_0)} a_0^{g_{+}}, \quad (24)$$

$$a_0^{\tilde{h}_{\perp}} = \frac{\phi_{\tilde{h}_{\perp}}(t_0)}{\phi_{\tilde{h}_{+}}(t_0)} a_0^{\tilde{h}_{+}}, \quad (25)$$

where the outer functions are evaluated using the physical masses. We enforce the endpoint constraints (5), (6), (7) by adding the term

$$\frac{(f_{+}(0) - f_0(0))^2}{\sigma_{\text{EP}}^2} + \frac{(g_{+}(0) - g_0(0))^2}{\sigma_{\text{EP}}^2} + \frac{(h_{\perp}(0) - \tilde{h}_{\perp}(0))^2}{\sigma_{\text{EP}}^2} \quad (26)$$

to the  $\chi^2$  function used in the fit, where the form factors are evaluated in the physical limit using Eq. (22), and  $\sigma_{\text{EP}}$  was set to  $5 \cdot 10^{-5}$ . Because the form factors at  $q^2 = 0$  depend on all  $z$ -expansion coefficients, this method is more convenient than parameter elimination, due to the additional asymptotic-behavior constraints discussed in the following.

A known problem with BGL-type  $z$  expansions is that the asymptotic behavior of the outer functions allows the form factors to grow for  $q^2 \rightarrow -\infty$  ( $z \rightarrow 1$ ), which is inconsistent with the expectation from perturbative QCD [120]. Given the outer functions from Ref. [117], we find that the parametrization (22) behaves, for  $q^2 \rightarrow -\infty$ , like

<sup>1</sup> Except for the  $B^*$ , whose masses we evaluate by adding a fixed hyperfine splitting of 45 MeV to the lattice  $B$  masses.

a polynomial containing the powers  $\{-q^2, \sqrt{-q^2}, 1, \frac{1}{\sqrt{-q^2}}, \dots\}$  for the form factors  $f_+$ ,  $g_+$ ,  $h_\perp$ , and  $\tilde{h}_\perp$ , and like a polynomial containing  $\{\sqrt{-q^2}, 1, \frac{1}{\sqrt{-q^2}}, \dots\}$  for the remaining form factors. We therefore impose sum rules on the coefficients  $a_n^f$  [118, 121, 122] such that the form factors must fall off at least like  $1/(-q^2)$  for  $q^2 \rightarrow -\infty$ , which matches the asymptotic behavior of the standard BCL-type  $z$  expansion [120] as used in Refs. [75, 95]. The asymptotic behavior of heavy-to-light baryon form factors was studied, for example, in Refs. [61, 62, 64, 123, 124], which predict even faster fall-off at the perturbative orders considered. To implement these sum rules, we follow Ref. [118] and solve for the coefficients  $\{a_{N+1}^f, a_{N+2}^f, a_{N+3}^f, a_{N+4}^f\}$  (in the case of  $f_+$ ,  $g_+$ ,  $h_\perp$ , and  $\tilde{h}_\perp$ ) and  $\{a_{N+1}^f, a_{N+2}^f, a_{N+3}^f\}$  (in the case of the other form factors) in terms of the lower-order coefficients  $\{a_0^f, a_1^f, \dots, a_N^f\}$ ; correspondingly in Eqs. (21) and (22), we set  $M = 4$  for  $f_+$ ,  $g_+$ ,  $h_\perp$ , and  $\tilde{h}_\perp$ , and  $M = 3$  for the other form factors. The explicit expressions for the eliminated higher-order coefficients are given in Appendix C.

Unlike in earlier determinations of  $\Lambda_b$ -decay form factors [75, 95], here we do not perform separate “nominal” and “higher-order” fits, and instead directly use a “higher-order” fit to obtain the physical-limit form factors. This has the advantage that the resulting covariance matrix of the fit parameters directly gives the total (statistical plus systematic) uncertainties. Moreover, instead of truncating the  $z$ -expansion at  $N = 2$ , with ad-hoc priors on the sizes of the second-order coefficients  $a_2^f$ , we now use dispersive bounds on the full set of  $z$ -expansion coefficients [116–118], and increase  $N$  until the central values and uncertainties of the physical-limit form factors stabilize in the full semileptonic region  $0 \leq q^2 \leq q_{\text{max}}^2$ . Our final results use  $N = 5$ . More details on this procedure are given farther below.

Among the parameters describing the pion-mass and lattice-spacing dependence,  $c_0^f$ ,  $c_1^f$ ,  $b^f$ , and  $d^f$  were left unconstrained, while the higher-order parameters  $\tilde{c}_0^f$ ,  $\tilde{b}^f$ ,  $\tilde{d}^f$ ,  $\tilde{d}^f$ , and  $j^f$ , which are not needed to describe the data, were constrained with Gaussian priors with central values and widths as in Eqs. (40)–(48) of Ref. [75]. By including these higher-order terms with priors limiting them to be not unnaturally large, systematic uncertainties from such higher-order effects are incorporated in the final form-factor results.

Besides the effects of the higher-order pion-mass and lattice-spacing terms, our fit also incorporates the following sources of systematic uncertainty:

1. When renormalizing the vector and axial-vector currents, the bootstrap samples for the quantities  $R_f$  [e.g., Eq. (16)] were generated with the residual matching factors and the  $\mathcal{O}(a)$ -improvement coefficients drawn from Gaussian random distributions, with central values and widths given in Table IV. Furthermore, in the data covariance matrix used for the fit, we included an additional 1% renormalization uncertainty for both the vector and axial-vector form factors to more conservatively account for missing higher-order corrections to the residual matching factors  $\rho_\Gamma$ ; this uncertainty is taken to be 100% correlated between either the vector or axial-vector form factors.
2. For the tensor form factors, the renormalization uncertainty is dominated by the use of the tree-level values,  $\rho_{T^{\mu\nu}} = 1$ , for the residual matching factors in the mostly nonperturbative renormalization procedure. Following Ref. [75], we estimate the systematic uncertainty in  $\rho_{T^{\mu\nu}}$  to be equal to 2 times the maximum value of  $|\rho_{V^\mu} - 1|$ ,  $|\rho_{A^\mu} - 1|$ , which is equal to 0.05316. Note that  $\rho_{T^{\mu\nu}}$  for the tensor current is scale-dependent, and our estimate of the matching uncertainty (and the values of the form factors themselves) should be interpreted as corresponding to  $\mu = 4.2$  GeV. To incorporate the tensor-current matching uncertainty in the fit, we introduced nuisance parameters multiplying the tensor form factors, with Gaussian priors equal to  $1 \pm 0.05316$ .
3. In Refs. [95, 97], the finite-volume errors in the  $\Lambda_b \rightarrow N$  and  $\Lambda_c \rightarrow N$  form factors were estimated to be 3% for the smallest value of  $m_\pi L$  used there. It is reasonable to expect similar behavior for the  $\Xi_b \rightarrow \Xi$  form factors. However, the smallest value of  $m_\pi L$  is larger here, and we therefore rescale the above estimate with the exponential of the ratio of the smallest  $m_\pi L$ , leading to an estimate of 1%. The isospin breaking effects are again estimated to be  $\mathcal{O}((m_d - m_u)/\Lambda_{\text{QCD}}) \approx 0.5\%$ , and  $\mathcal{O}(\alpha_{\text{e.m.}}) \approx 0.7\%$ . The finite-volume and isospin-breaking uncertainties were added to the data covariance matrix used in the fit, assuming 100% correlation within either the vector, axial-vector, and tensor form factors.
4. The uncertainties in the lattice spacings and pion masses were included by promoting these values to fit parameters with Gaussian priors determined by the central values and uncertainties listed in Table I.

For the parametrization (22), the dispersive bound takes the form<sup>2</sup> [117, 118]

$$D_{f_0} \leq 1, D_{f_{+,\perp}} \leq 1, D_{g_0} \leq 1, D_{g_{+,\perp}} \leq 1, D_{h_{+,\perp}} \leq 1, D_{\tilde{h}_{+,\perp}} \leq 1, \quad (27)$$

<sup>2</sup> We do not include the one-particle contributions due to the  $B_s$  bound states here.

$f$	$J^P$	$m_{\text{pole}}^f$ [GeV]
$f_+, f_\perp, h_+, h_\perp,$	$1^-$	5.416
$f_0$	$0^+$	5.711
$g_+, g_\perp, \tilde{h}_+, \tilde{h}_\perp,$	$1^+$	5.750
$g_0$	$0^-$	5.367

TABLE VI.  $B_s$  meson poles in each of the different form factors.

where

$$D_{f_0} = \sum_{n=0}^{N+3} \sum_{n'=0}^{N+3} a_n^{f_0} \langle z^n | z^{n'} \rangle_{\alpha_V} a_{n'}^{f_0}, \quad (28)$$

$$D_{f_{+,\perp}} = \sum_{n=0}^{N+4} \sum_{n'=0}^{N+4} a_n^{f_{+,\perp}} \langle z^n | z^{n'} \rangle_{\alpha_V} a_{n'}^{f_{+,\perp}} + \sum_{n=0}^{N+3} \sum_{n'=0}^{N+3} a_n^{f_{+,\perp}} \langle z^n | z^{n'} \rangle_{\alpha_V} a_{n'}^{f_{+,\perp}}, \quad (29)$$

$$D_{g_0} = \sum_{n=0}^{N+3} \sum_{n'=0}^{N+3} a_n^{g_0} \langle z^n | z^{n'} \rangle_{\alpha_A} a_{n'}^{g_0}, \quad (30)$$

$$D_{g_{+,\perp}} = \sum_{n=0}^{N+4} \sum_{n'=0}^{N+4} a_n^{g_{+,\perp}} \langle z^n | z^{n'} \rangle_{\alpha_A} a_{n'}^{g_{+,\perp}} + \sum_{n=0}^{N+3} \sum_{n'=0}^{N+3} a_n^{g_{+,\perp}} \langle z^n | z^{n'} \rangle_{\alpha_V} a_{n'}^{g_{+,\perp}}, \quad (31)$$

$$D_{h_{+,\perp}} = \sum_{n=0}^{N+3} \sum_{n'=0}^{N+3} a_n^{h_{+,\perp}} \langle z^n | z^{n'} \rangle_{\alpha_V} a_{n'}^{h_{+,\perp}} + \sum_{n=0}^{N+4} \sum_{n'=0}^{N+4} a_n^{h_{+,\perp}} \langle z^n | z^{n'} \rangle_{\alpha_V} a_{n'}^{h_{+,\perp}}, \quad (32)$$

$$D_{\tilde{h}_{+,\perp}} = \sum_{n=0}^{N+3} \sum_{n'=0}^{N+3} a_n^{\tilde{h}_{+,\perp}} \langle z^n | z^{n'} \rangle_{\alpha_A} a_{n'}^{\tilde{h}_{+,\perp}} + \sum_{n=0}^{N+4} \sum_{n'=0}^{N+4} a_n^{\tilde{h}_{+,\perp}} \langle z^n | z^{n'} \rangle_{\alpha_A} a_{n'}^{\tilde{h}_{+,\perp}}, \quad (33)$$

with

$$\langle z^n | z^{n'} \rangle_\alpha = \begin{cases} \frac{\sin(\alpha(n-n'))}{\pi(n-n')}, & n \neq n', \\ \frac{\pi}{\alpha}, & n = n', \end{cases} \quad (34)$$

and

$$\alpha_V = \arg z((m_{\Xi_b} + m_\Xi)^2, t_0, (m_B + m_K)^2) \approx 1.43829, \quad (35)$$

$$\alpha_A = \arg z((m_{\Xi_b} + m_\Xi)^2, t_0, (m_{B^*} + m_K)^2) \approx 1.47256. \quad (36)$$

To implement the dispersive bounds, we use the algorithm proposed in Ref. [118], which we apply directly to the fit of the lattice data using Eq. (21):

1. We perform a fit using Eq. (21) in which the following term is added to the  $\chi^2$  function:

$$\left( D_{f_0} + D_{f_{+,\perp}} + D_{g_0} + D_{g_{+,\perp}} + D_{h_{+,\perp}} + D_{\tilde{h}_{+,\perp}} \right) / \sigma_D^2, \quad (37)$$

where  $\sigma_D$  is an arbitrary width of order 1 that can be tuned to optimize the efficiency of the algorithm (we use  $\sigma_D = 0.5$ ).

2. We generate a large number ( $\sim 10^6$  to  $10^8$ , depending on  $N$ ) of multivariate Gaussian random samples for the  $10(N+1) - 2$   $z$ -expansion coefficients that are actual fit parameters, with mean given by the best fit point and covariance matrix computed using the Hessian of  $\chi^2$  at the best-fit point.

$f$	$a_0^f$	$a_1^f$	$a_2^f$	$a_3^f$	$a_4^f$	$a_5^f$
$f_0$	$0.0749 \pm 0.0027$	$-0.574 \pm 0.063$	$2.90 \pm 0.77$	$-8.9 \pm 4.4$	$16 \pm 11$	$-19 \pm 16$
$f_+$	$0.0307 \pm 0.0010$	$-0.265 \pm 0.022$	$1.33 \pm 0.31$	$-4.0 \pm 2.3$	$8 \pm 7$	$-10 \pm 14$
$f_\perp$	$0.0771 \pm 0.0025$	$-0.571 \pm 0.050$	$2.34 \pm 0.58$	$-5.7 \pm 3.6$	$9 \pm 10$	$-9 \pm 14$
$g_0$	$0.0900 \pm 0.0035$	$-0.700 \pm 0.077$	$3.06 \pm 0.80$	$-7.1 \pm 4.2$	$10 \pm 11$	$-9 \pm 15$
$g_+$	$0.0186 \pm 0.0006$	$-0.148 \pm 0.014$	$0.73 \pm 0.22$	$-2.2 \pm 1.6$	$4 \pm 5$	$-5 \pm 9$
$g_\perp$		$-0.412 \pm 0.040$	$1.95 \pm 0.52$	$-4.4 \pm 3.2$	$5 \pm 8$	$-4 \pm 12$
$h_+$	$0.0630 \pm 0.0039$	$-0.386 \pm 0.047$	$1.01 \pm 0.52$	$-1.6 \pm 3.4$	$2 \pm 9$	$-1 \pm 14$
$h_\perp$	$0.0468 \pm 0.0030$	$-0.367 \pm 0.041$	$1.52 \pm 0.48$	$-3.6 \pm 3.3$	$5 \pm 11$	$-5 \pm 19$
$\tilde{h}_+$	$0.0468 \pm 0.0029$	$-0.331 \pm 0.037$	$1.58 \pm 0.45$	$-4.1 \pm 3.0$	$6 \pm 8$	$-6 \pm 12$
$\tilde{h}_\perp$		$-0.251 \pm 0.027$	$1.33 \pm 0.36$	$-4.8 \pm 2.6$	$11 \pm 8$	$-16 \pm 15$

TABLE VII. Mean values and standard deviations of the accepted samples for the  $z$ -expansion parameters. Machine-readable files containing these values and their covariance matrix with more digits are provided in the supplemental material [125]. The parameters  $a_0^{g_\perp}$  and  $a_0^{\tilde{h}_\perp}$ , as well as  $\{a_6^f, a_7^f, a_8^f, a_9^f\}$  for  $f \in \{f_+, g_+, h_\perp, \tilde{h}_\perp\}$  and  $\{a_6^f, a_7^f, a_8^f\}$  for  $f \in \{f_0, f_\perp, g_0, g_\perp, h_+, \tilde{h}_+\}$ , must be determined from these parameters using Eqs. (24), (25), (C10-C13), (C17-C19).

3. For each sample, we check whether the dispersive bound (27) is satisfied [this requires computing the derived coefficients  $a_0^{g_\perp}$ ,  $a_0^{\tilde{h}_\perp}$ , and  $\{a_{N+1}^f, \dots, a_{N+M}^f\}$  using Eqs. (24), (25), (C10-C13), (C17-C19)]. If not, the sample is discarded. If yes, we draw a single uniformly distributed random number  $p \in [0, 1]$ . We then accept the sample if

$$p \leq \frac{\exp[-3/\sigma_D^2]}{\exp\left[\left(D_{f_0} + D_{f_{+, \perp}} + D_{g_0} + D_{g_{+, \perp}} + D_{h_{+, \perp}} + D_{\tilde{h}_{+, \perp}}\right)/(2\sigma_D^2)\right]}. \quad (38)$$

One can then compute the observable of interest (such as the value of a form factor, or a decay rate depending on the form factors) for each of the accepted samples to obtain the probability distribution for the observable. We have done this for the values of the form factors at  $q^2 = 0$  and  $q^2 = q_{\max}^2$  and found that the distributions are reasonably close to Gaussian, and it is sufficient to instead evaluate the form factors using the mean vector of the accepted parameter samples, and evaluate their uncertainty with derivative-based error propagation using the covariance matrix of the  $z$ -expansion parameters computed from the accepted samples. We have performed the analysis for different  $z$ -expansion orders up to  $N = 6$ , and found that the central values and uncertainties of the form factors at  $q^2 = 0$  (which, in the semileptonic region, is the point with the highest sensitivity to  $N$ , as it corresponds to the farthest extrapolation of the lattice data) stabilize at  $N = 5$  and are practically unchanged when going to  $N = 6$ . Therefore, we choose the  $N = 5$  results as our final results. In the Supplemental Material [125], we provide machine-readable files containing, for the 58  $z$ -expansion fit parameters,

1. The 4350 accepted samples (out of 20,000,000 initial samples) from the above procedure,
2. The mean vector and covariance matrix of the accepted samples,
3. The best-fit values and covariance matrix from the initial fit in step 1 above. These are included for reproducibility and possibly different statistical processing, and should not be used directly in phenomenological applications.

The mean vector and standard deviations of the accepted samples are also listed in Table VII. Plots of the chiral-continuum extrapolations of the form factors are shown in Figs. 4, 5, 6, and 7. The physical-limit curves were evaluated using the mean vector and covariance matrix of the accepted samples.

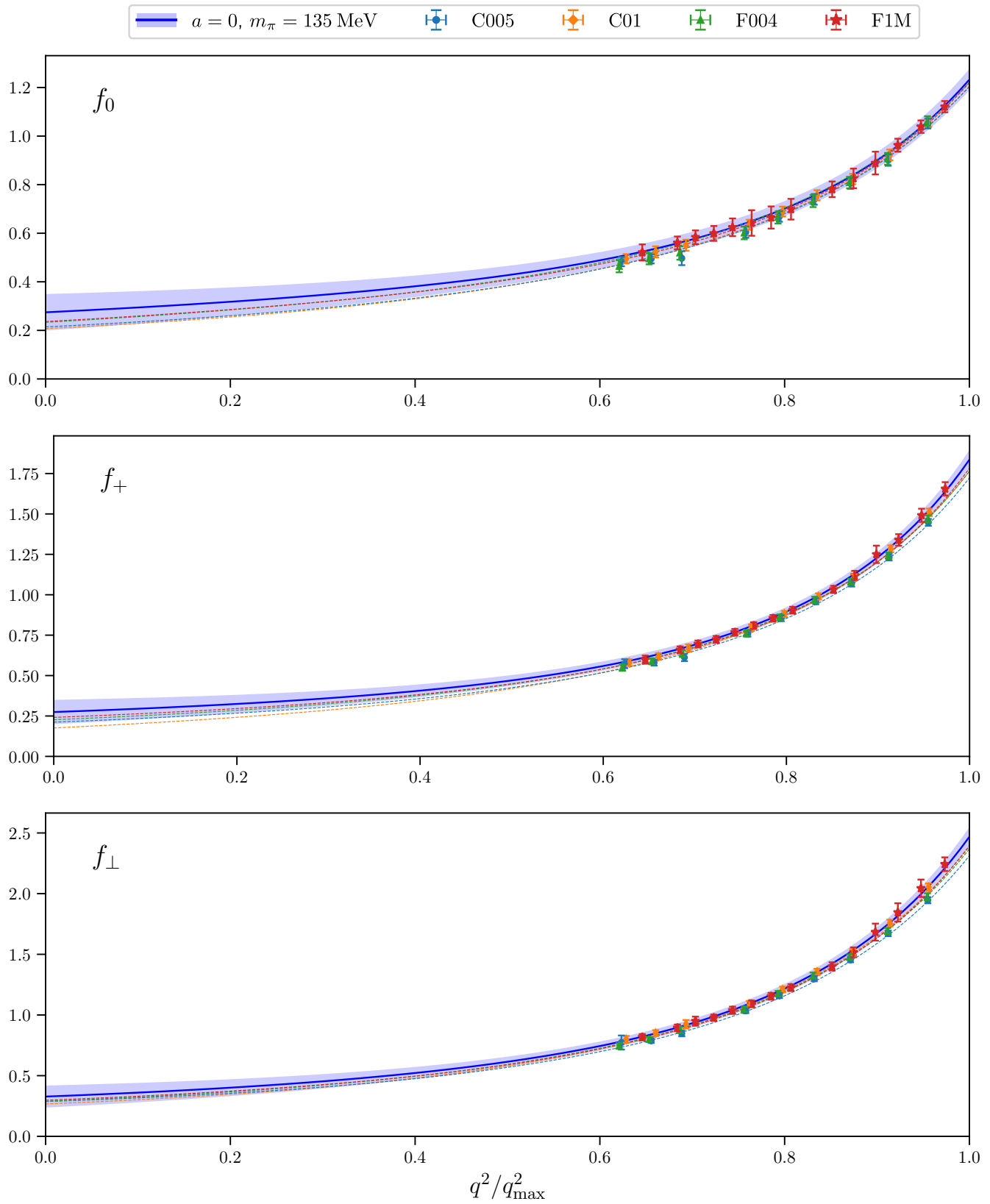


FIG. 4. Chiral and continuum extrapolations of the  $\Xi_b \rightarrow \Xi$  vector form factors. The solid blue lines show the form factor curves in the physical limit, while the dashed lines show the modified  $z$ -expansion fits evaluated with the individual lattice spacings and pion masses for each ensemble. The bands include the combined statistical and systematic uncertainties.

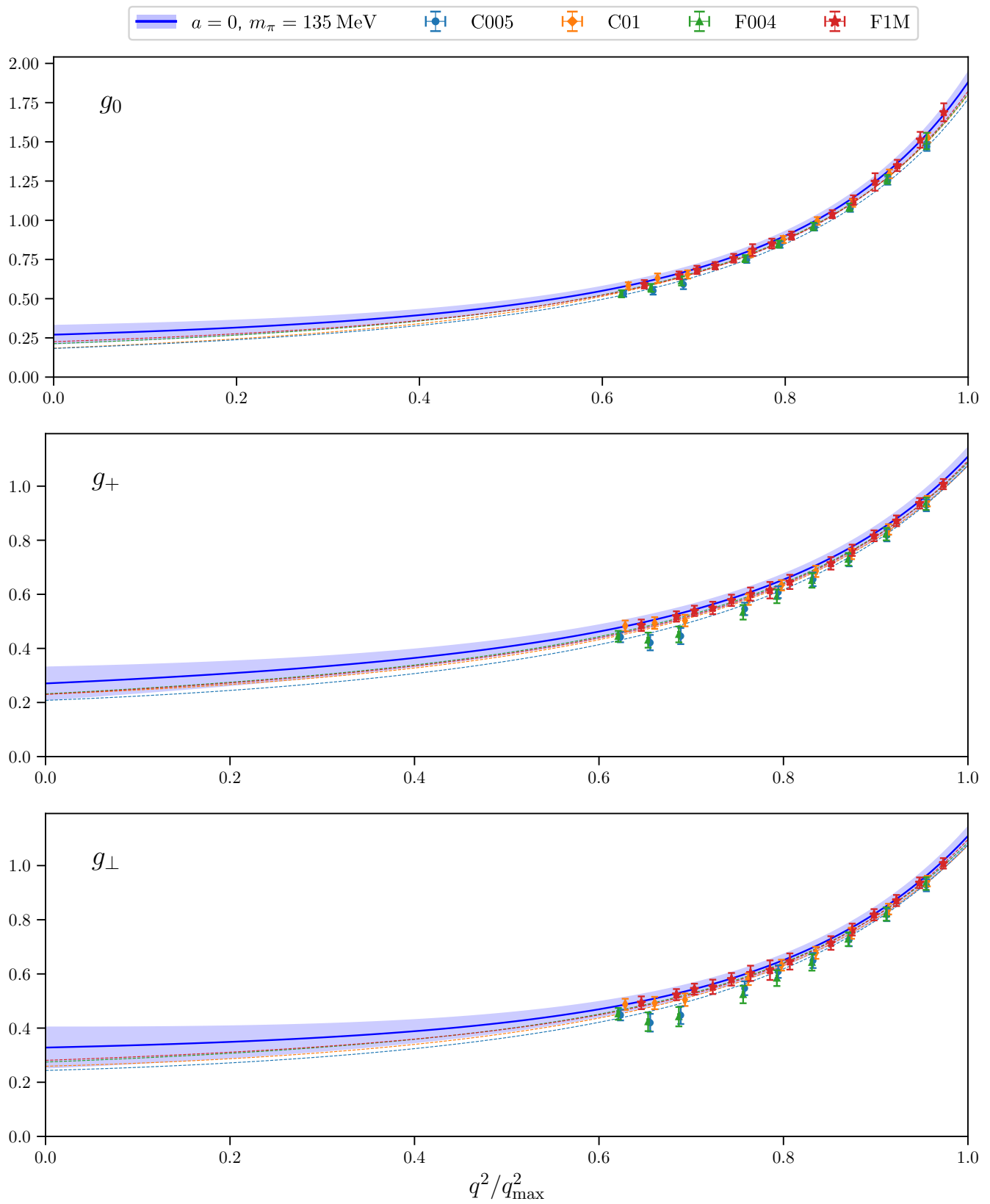


FIG. 5. Like Fig. 4, but for the axial-vector form factors.

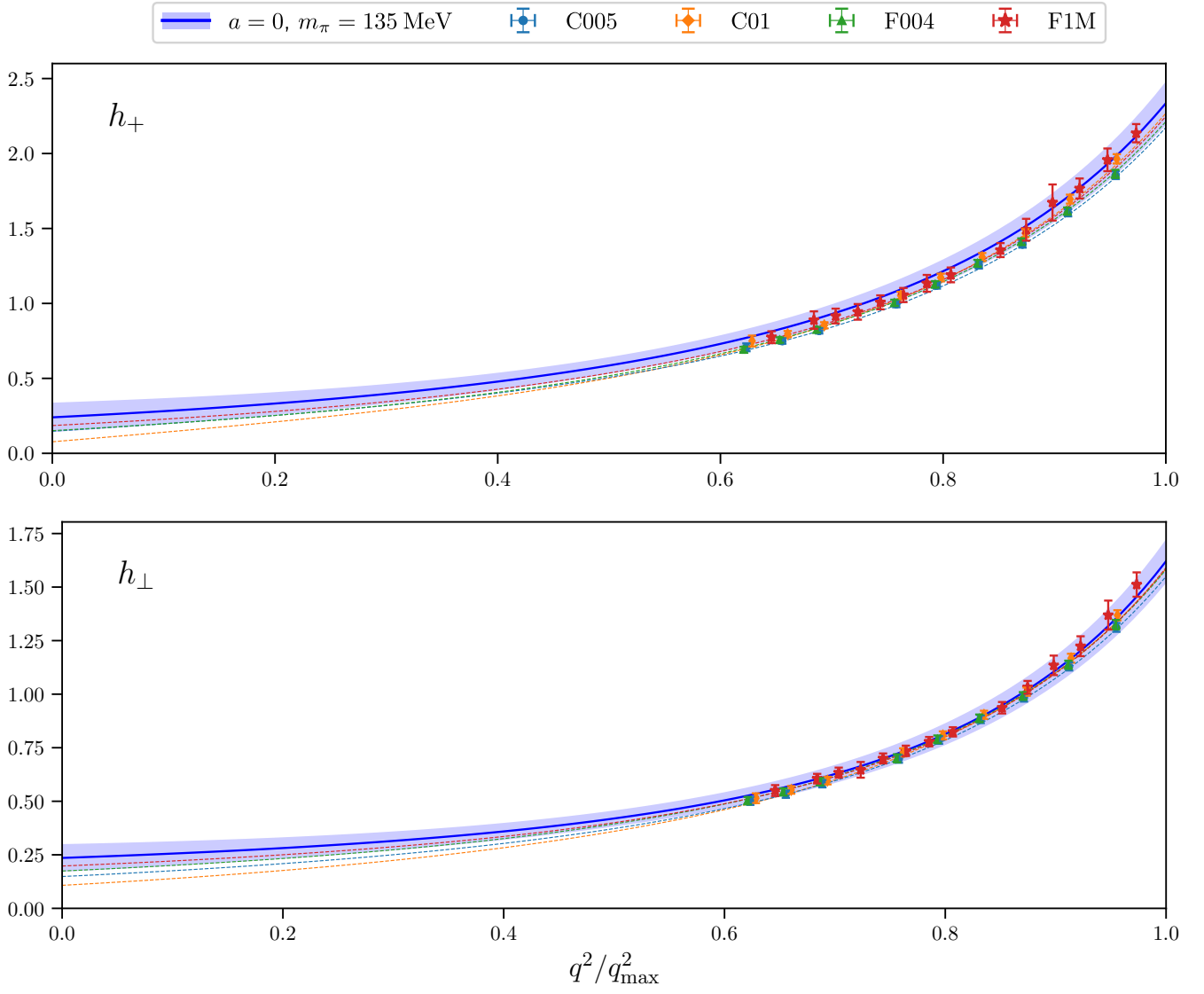


FIG. 6. Like Fig. 4, but for the tensor form factors  $h_+$  and  $h_\perp$ .

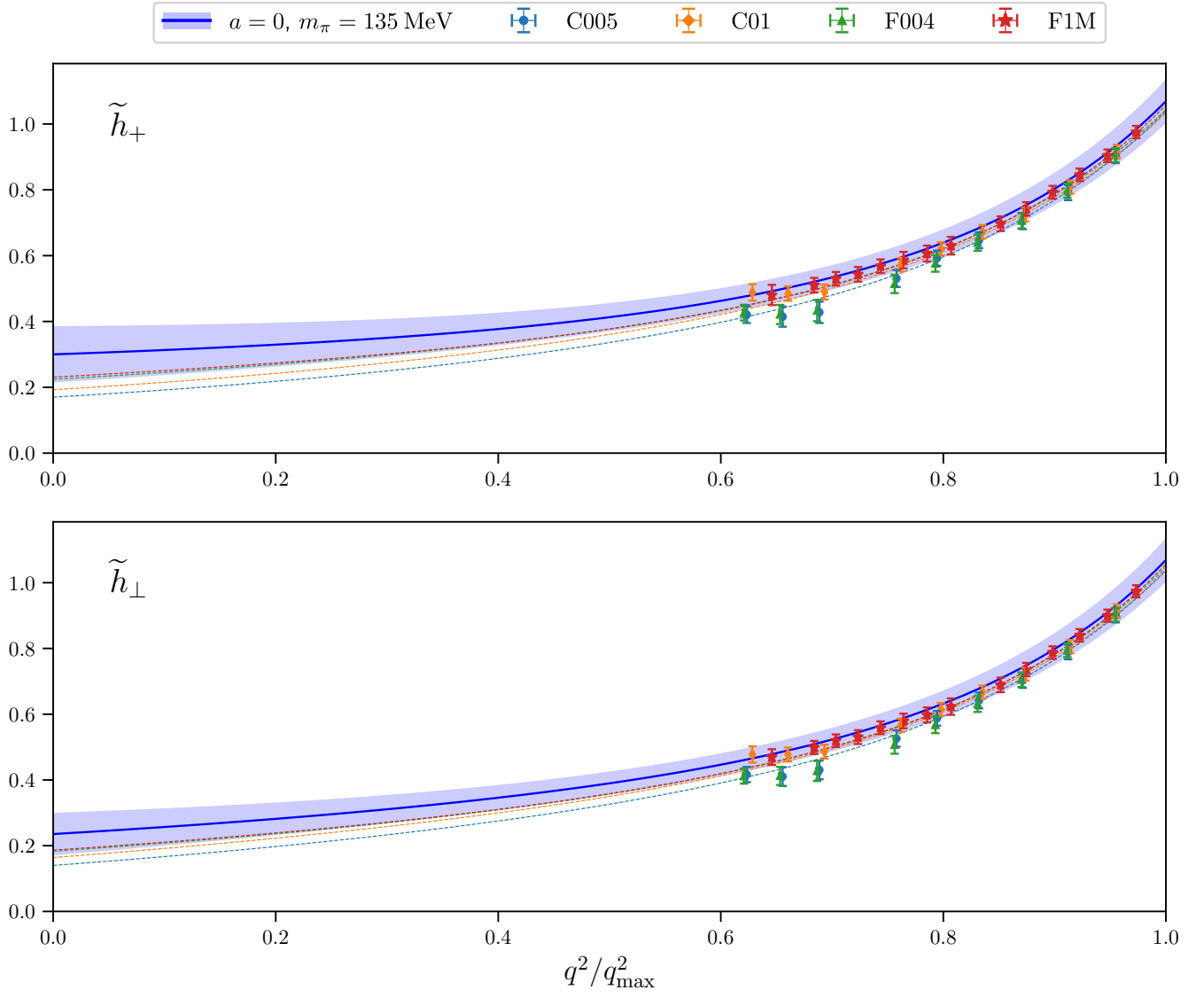


FIG. 7. Like Fig. 4, but for the tensor form factors  $\tilde{h}_+$  and  $\tilde{h}_\perp$ .

## V. STANDARD-MODEL PREDICTIONS FOR $\Xi_b^- \rightarrow \Xi^- \mu^+ \mu^-$ AND $\Xi_b^- \rightarrow \Xi^- \gamma$ DECAYS

To predict the  $\Xi_b^- \rightarrow \Xi^- \mu^+ \mu^-$  differential branching fraction and angular observables in the Standard Model, we closely follow Ref. [75] (and references therein), which considered  $\Lambda_b \rightarrow \Lambda \mu^+ \mu^-$ . Here, we do not include the secondary decay of the  $\Xi^-$  and calculate only the two-fold decay distribution

$$\frac{d^2\Gamma}{dq^2 d\cos\theta_\ell} = \frac{3}{2} (K_{1ss} \sin^2\theta_\ell + K_{1cc} \cos^2\theta_\ell + K_{1c} \cos\theta_\ell), \quad (39)$$

where  $\theta_\ell$  is the polar angle of the negatively charged lepton [45]. The integral over  $\cos\theta_\ell$  gives the  $q^2$ -differential decay rate

$$\frac{d\Gamma}{dq^2} = 2K_{1ss} + K_{1cc}. \quad (40)$$

The two specific angular observables we consider are

$$F_L = 2\widehat{K}_{1ss} - \widehat{K}_{1cc}, \quad (41)$$

$$A_{FB}^\ell = \frac{3}{2}\widehat{K}_{1c}, \quad (42)$$

where  $\widehat{K}_i = K_i/(d\Gamma/dq^2)$ . We limit our predictions to the kinematic regions  $q^2 < 8 \text{ GeV}^2$  and  $q^2 > 15 \text{ GeV}^2$  to avoid the effects of narrow charmonium resonances, and use the approximation in which all nonlocal hadronic matrix elements are reduced to local matrix elements through the effective Wilson coefficients  $C_7^{\text{eff}}(q^2)$  and  $C_9^{\text{eff}}(q^2)$ , given in Eqs. (65) and (66) of Ref. [75] (following Ref. [126]), which are based on Refs. [127–131]. We take the Standard-Model expressions for the functions  $K_i$  in this approximation, and including lepton-mass effects, from Eqs. (A1) and (A2) of Ref. [65] (with the appropriate replacements of the baryon masses, and using the form-factor relations given in Ref. [75]). To evaluate the  $\Xi_b \rightarrow \Xi$  form factors, we use the mean values and covariance matrix of the accepted samples (cf. Sec. IV) of the  $z$ -expansion coefficients. The values we use for the Wilson coefficients  $C_1$ – $C_{10}$ , the  $b$ -quark mass, and the strong and electromagnetic couplings are given in Table VIII; the pole masses that enter in  $C_7^{\text{eff}}(q^2)$  and  $C_9^{\text{eff}}(q^2)$  are

$$m_c^{\text{pole}} = 1.6030 \text{ GeV}, \quad (43)$$

$$m_b^{\text{pole}} = 4.7231 \text{ GeV}. \quad (44)$$

We evaluated all of these as in Ref. [75], and, except for  $\alpha_e$ , updated them using EOS [132] with the latest Standard-Model input parameters from Ref. [119]. We further take

$$|V_{ts}^* V_{tb}| = 0.04113 \pm 0.00036 \quad (45)$$

	$\mu = 2.1 \text{ GeV}$	$\mu = 4.2 \text{ GeV}$	$\mu = 8.4 \text{ GeV}$
$C_1$	−0.4996	−0.2891	−0.1494
$C_2$	1.0248	1.0102	1.0036
$C_3$	−0.0145	−0.0061	−0.0027
$C_4$	−0.1517	−0.0866	−0.0546
$C_5$	0.0010	0.0004	0.0002
$C_6$	0.0033	0.0011	0.0004
$C_7$	−0.3786	−0.3362	−0.3035
$C_8$	−0.2133	−0.1823	−0.1630
$C_9$	4.5589	4.2665	3.8628
$C_{10}$	−4.1333	−4.1133	−4.1333
$m_b^{\overline{\text{MS}}} [\text{GeV}]$	4.9021	4.1737	3.7239
$\alpha_s$	0.2972	0.2248	0.1860
$\alpha_e$	1/134.44	1/133.28	1/132.51

TABLE VIII. Wilson coefficients,  $b$ -quark mass, and strong and electromagnetic couplings in the  $\overline{\text{MS}}$  scheme at the nominal scale  $\mu = 4.2 \text{ GeV}$  and at the low and high scales used to estimate the perturbative uncertainties.

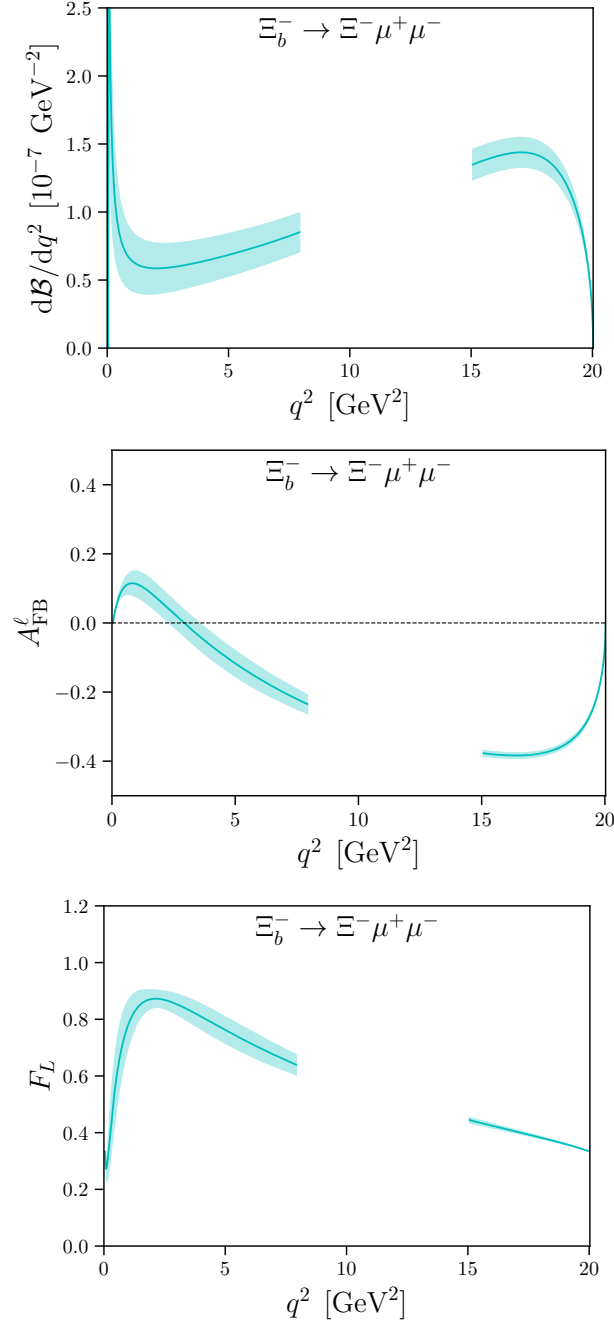


FIG. 8. Standard-Model predictions for the  $\Xi_b^- \rightarrow \Xi^- \mu^+ \mu^-$  differential branching fraction and the angular observables  $F_L$  and  $A_{FB}^\ell$ .

from UTFit [133] and, to evaluate the differential branching fraction  $d\mathcal{B}/dq^2 = \tau_{\Xi_b^-} d\Gamma/dq^2$ ,

$$\tau_{\Xi_b^-} = (1.570 \pm 0.023) \text{ ps} \quad (46)$$

from Ref. [119]. The resulting Standard-Model predictions are shown as a function of  $q^2$  in Fig. 8; in addition, we provide predictions for selected  $q^2$  bins in Table IX. For the angular observables, the numerator and denominator of  $\widehat{K}_i = K_i/(d\Gamma/dq^2)$  are binned first before taking the ratio.

For the radiative decay  $\Xi_b^- \rightarrow \Xi^- \gamma$ , we again use the approximation in which nonlocal hadronic matrix elements

	$\langle d\mathcal{B}/dq^2 \rangle$	$\langle F_L \rangle$	$\langle A_{\text{FB}}^\ell \rangle$
[0.1, 2]	0.77(27)	0.65(11)	0.088(25)
[1.1, 6]	0.64(17)	0.811(41)	-0.038(39)
[2, 4]	0.61(18)	0.849(38)	-0.005(41)
[4, 6]	0.69(16)	0.762(49)	-0.117(40)
[6, 8]	0.79(15)	0.675(43)	-0.202(33)
[15, 16]	1.377(98)	0.435(11)	-0.380(10)
[16, 18]	1.426(93)	0.404(82)	-0.3793(94)
[18, 20]	1.083(73)	0.3634(42)	-0.3087(98)
[15, 20]	1.279(83)	0.3967(73)	-0.3556(93)

TABLE IX. Standard-Model predictions for the binned  $\Xi_b^- \rightarrow \Xi^- \mu^+ \mu^-$  differential branching fraction (in units of  $10^{-7} \text{ GeV}^{-2}$ ) and angular observables (with unpolarized  $\Xi_b$ ). The first column specifies the bin ranges  $[q_{\text{min}}^2, q_{\text{max}}^2]$  in units of  $\text{GeV}^2$ .

are rewritten as local matrix elements via  $C_7^{\text{eff}}(q^2 = 0)$ , such that (see, e.g., Ref. [65])

$$\mathcal{B}(\Xi_b^- \rightarrow \Xi^- \gamma) = \tau_{\Xi_b^-} \alpha_e \left( \frac{G_F |V_{ts}^* V_{tb}| m_b^{\overline{\text{MS}}} |C_7^{\text{eff}}(0)|}{4\pi^2 \sqrt{2}} \right)^2 \frac{(m_{\Xi_b^-}^2 - m_{\Xi^-}^2)^3}{m_{\Xi_b^-}^3} h_\perp(0)^2, \quad (47)$$

where we used the endpoint relation (7). For  $C_7^{\text{eff}}(0)$ , we again use Eq. (65) of Ref. [75], which, at  $\mu = 4.2 \text{ GeV}$  is found to be

$$C_7^{\text{eff}}(0) \approx -0.36795 - 0.01355 i. \quad (48)$$

We obtain the Standard-Model prediction

$$\mathcal{B}(\Xi_b^- \rightarrow \Xi^- \gamma) = (2.9 \pm 1.6) \times 10^{-5}. \quad (49)$$

For all observables computed in this section, the uncertainties given include the form-factor and parametric uncertainties, the perturbative uncertainties, estimated as the change in the observable when varying the renormalization scale from  $\mu = 2.1 \text{ GeV}$  to  $\mu = 8.4 \text{ GeV}$ , and, following Ref. [75], an additional 5% uncertainty assigned to  $C_7^{\text{eff}}(q^2)$  and  $C_9^{\text{eff}}(q^2)$  in an attempt to account for some of the approximations used for the nonlocal matrix elements. Our analysis neglects nonfactorizable effects, whose theory for baryonic decays is only partially developed (see Ref. [38] for recent progress).

## VI. CONCLUSIONS

This work is the first lattice QCD calculation of  $\Xi_b \rightarrow \Xi$  form factors, and also introduces an important methodological advance in lattice QCD calculations of  $b$ -baryon decay form factors: the use of dispersive bounds in the chiral-continuum-kinematic extrapolations, which has allowed us to increase the order of the  $z$  expansion until the values and uncertainties of the extrapolated form factors stabilize, thereby achieving controlled uncertainties in the full semileptonic kinematic range. In the high- $q^2$  region, our final results in the continuum limit and at the physical pion mass have uncertainties of approximately 3-4% for the vector and axial-vector form factors, and approximately 6-7% for the tensor form factors. At  $q^2 = 0$ , the uncertainties in all form factors are on the order of 25%.

If  $SU(3)$  flavor symmetry was exact, the  $\Xi_b \rightarrow \Xi$  form factors would be equal to the  $\Lambda_b \rightarrow p$  form factors, and equal to  $\sqrt{3/2}$  times the  $\Lambda_b \rightarrow \Lambda$  form factors. A comparison with the QCD lattice results for  $\Lambda_b \rightarrow p$  [95] and  $\Lambda_b \rightarrow \Lambda$  [75] shows that these relations are indeed satisfied up to the expected natural size of  $SU(3)$  symmetry breaking.

Comparisons of our results for the  $\Xi_b \rightarrow \Xi$  form factors with continuum calculations are shown in Tables X and XI at the kinematic points  $q^2 = q_{\text{max}}^2$  and  $q^2 = 0$ . Compared to Rui *et al.*, 2025 [85], the central values of our results tend to be lower, but there is a reasonable overall agreement given the estimated uncertainties. A larger number of continuum calculations are available for the tensor form factor at  $q^2 = 0$  that is relevant for the  $\Xi_b \rightarrow \Xi \gamma$  decay rates, as shown in Table XI. The quark models of Refs. [91] and [90] gave lower values for this form factor compared to our lattice calculation, while Refs. [85] and especially Ref. [93] gave higher values.

Our Standard-Model prediction for  $\mathcal{B}(\Xi_b^- \rightarrow \Xi^- \gamma)$  is consistent with the upper bound  $\mathcal{B}(\Xi_b^- \rightarrow \Xi^- \gamma) < 1.3 \times 10^{-4}$  from LHCb [87] and with the previous Standard-Model predictions shown in Table XI, except for that of Ref. [93],

	This work	Rui <i>et al.</i> , 2025 [85]	Azizi <i>et al.</i> , 2011 [81]
$f_0(q_{\max}^2)$	$1.233 \pm 0.045$	$1.525_{-0.087-0.115-0.063}^{+0.005+0.010+0.000}$	-0.060
$f_+(q_{\max}^2)$	$1.837 \pm 0.060$	$2.391_{-0.054-0.039-0.137}^{+0.058+0.137+0.045}$	1.628
$f_{\perp}(q_{\max}^2)$	$2.469 \pm 0.080$	$3.019_{-0.034-0.156-0.184}^{+0.102+0.076+0.104}$	3.667
$g_0(q_{\max}^2)$	$1.881 \pm 0.072$	$2.060_{-0.066-0.000-0.370}^{+0.022+0.140+0.213}$	2.987
$g_+(q_{\max}^2) = g_{\perp}(q_{\max}^2)$	$1.109 \pm 0.038$	$1.144_{-0.108-0.000-0.296}^{+0.036+0.134+0.165}$	0.825
$h_+(q_{\max}^2)$	$2.34 \pm 0.14$	$3.815_{-0.709-1.391-0.881}^{+0.000+0.000+0.000}$	
$h_{\perp}(q_{\max}^2)$	$1.62 \pm 0.10$	$2.899_{-0.439-0.832-0.584}^{+0.000+0.000+0.000}$	
$\tilde{h}_+(q_{\max}^2) = \tilde{h}_{\perp}(q_{\max}^2)$	$1.069 \pm 0.067$	$1.181_{-0.002-0.062-0.060}^{+0.035+0.078+0.082}$	
$f_0(0) = f_+(0)$	$0.274 \pm 0.075$	$0.342_{-0.000-0.013-0.024}^{+0.008+0.013+0.018}$	0.142
$f_{\perp}(0)$	$0.328 \pm 0.091$	$0.457_{-0.000-0.017-0.031}^{+0.010+0.018+0.023}$	0.284
$g_0(0) = g_+(0)$	$0.270 \pm 0.063$	$0.354_{-0.000-0.016-0.020}^{+0.010+0.013+0.015}$	0.160
$g_{\perp}(0)$	$0.328 \pm 0.078$	$0.284_{-0.000-0.010-0.015}^{+0.005+0.012+0.012}$	0.120
$h_+(0)$	$0.240 \pm 0.098$	$0.429_{-0.000-0.000-0.009}^{+0.033+0.029+0.043}$	
$\tilde{h}_+(0)$	$0.300 \pm 0.086$	$0.282_{-0.000-0.009-0.018}^{+0.006+0.010+0.014}$	
$h_{\perp}(0) = \tilde{h}_{\perp}(0)$	$0.235 \pm 0.065$	$0.338_{-0.000-0.000-0.015}^{+0.015+0.009+0.024}$	

TABLE X. Comparison of our results for the form factors at  $q^2 = q_{\max}^2$  and  $q^2 = 0$  with those from Refs. [85] and [81]. Reference [85] provides separate values for  $h_{\perp}(0)$  and  $\tilde{h}_{\perp}(0)$  which are consistent with each other within the uncertainties; the value shown in the table is  $h_{\perp}(0)$ . In Ref. [81], the matrix elements of the tensor current are written in terms of six form factors, of which only four are independent. The numerical parameterizations given for the six tensor form factors violate the exact kinematical relations between these form factors, and therefore we only list the vector and axial-vector form factors from Ref. [81].

	Method	$h_{\perp}(0) = \tilde{h}_{\perp}(0)$	$\mathcal{B}(\Xi_b^- \rightarrow \Xi^- \gamma)$
LHCb, 2021 [87]	Experiment		$< 1.3 \times 10^{-4}$
This work	Lattice QCD	$0.235 \pm 0.065$	$(2.9 \pm 1.6) \times 10^{-5}$
Rui <i>et al.</i> , 2025 [85]	pQCD approach	$0.338_{-0.000-0.000-0.015}^{+0.015+0.009+0.024}$	
Aliev <i>et al.</i> , 2023 [92]	Light-cone sum rules	$0.31 \pm 0.04$	$(4.8 \pm 1.3) \times 10^{-5}$
Davydov <i>et al.</i> , 2022 [91]	Relativistic quark model	$0.144 \pm 0.007$	$(0.95 \pm 0.15) \times 10^{-5}$
Geng <i>et al.</i> , 2022 [90]	Light-front quark model	0.143	$(1.1 \pm 0.1) \times 10^{-5}$
Olamaei <i>et al.</i> , 2021 [89]	Light-cone sum rules [81]		$(1.08_{-0.49}^{+0.63}) \times 10^{-5}$
Wang <i>et al.</i> , 2021 [88]	Flavor- $SU(3)$ symmetry		$(1.23 \pm 0.64) \times 10^{-5}$
Liu <i>et al.</i> , 2011 [93]	Light-cone sum rules	$\approx 0.6$	$(3.03 \pm 0.10) \times 10^{-4}$

TABLE XI. Comparison of results for the tensor form factor  $h_{\perp}(0) = \tilde{h}_{\perp}(0)$  and of Standard-model predictions for the  $\Xi_b^- \rightarrow \Xi^- \gamma$  branching fraction. Also shown is the experimental upper bound on this branching fraction from LHCb. Note that the Flavor- $SU(3)$ -symmetry prediction [88] uses the LHCb experimental result for  $\mathcal{B}(\Lambda_b \rightarrow \Lambda \gamma)$  [86] as an input, and could therefore be directly affected by new physics.

which is about a factor 10 higher. Our Standard-Model prediction of the  $\Xi_b^- \rightarrow \Xi^- \mu^+ \mu^-$  differential branching fraction, shown in Fig. 8, has central values approximately 25% below the prediction of Ref. [85], but is consistent with Ref. [85] within the combined uncertainties. We look forward to future experimental results for this decay.

## ACKNOWLEDGMENTS

We are grateful to the RBC and UKQCD Collaborations for making their gauge-field ensembles available. We thank Enrico Lunghi for a discussion on the theory of  $b \rightarrow s\gamma$  decays. We acknowledge financial support by the U.S. Department of Energy, Office of Science, Office of High Energy Physics under Award Number DE-SC0009913. This research used resources of the National Energy Research Scientific Computing Center (NERSC), a U.S. Department of Energy Office of Science User Facility supported by Contract Number DE-AC02-05CH1123. This research also used resources at Purdue University RCAC and at the University of Texas TACC through the Extreme Science and Engineering Discovery Environment (XSEDE) [134] and the Advanced Cyberinfrastructure Coordination Ecosystem: Services & Support (ACCESS) program [135], which are supported by U.S. National Science Foundation grants ACI-154856, 2138259, 2138286, 2138307, 2137603, and 2138296. We acknowledge the use of Chroma [136, 137], QLUA [138], MDWF [139], and related USQCD software [140].

## DATA AVAILABILITY

Machine-readable files containing the accepted samples of the form-factor parameters, their mean and covariance matrix, as well as the central values and covariance matrix from the initial fit prior to the “reweighting” procedure, are provided in the Supplemental Material [125]. The other data are available from the authors upon reasonable request.

### Appendix A: Additional plots of ratio fits

This appendix contains sample plots of the ratio fits for the other ensembles (Fig. 9).

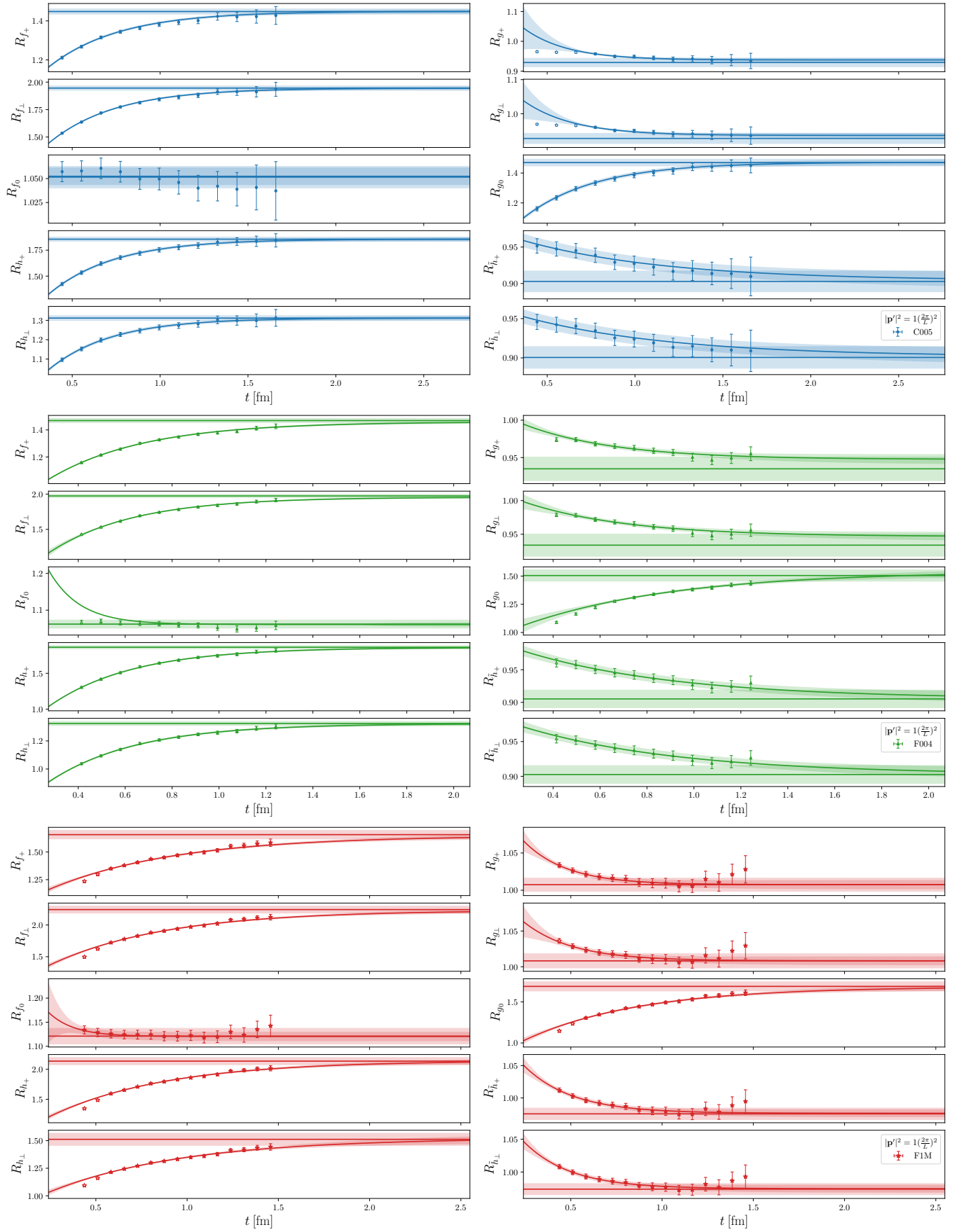


FIG. 9. Like Fig. 3, but for the other ensembles.

## Appendix B: Outer functions and susceptibilities

The outer functions are taken from Ref. [117] (with the appropriate replacements of the baryon masses), and are shown here in our different notation for convenience. Following Refs. [141, 142], the outer functions are compactly expressed as

$$\phi_f(q^2) = \frac{(m_{\Xi_b} + m_{\Xi})^{A_f} (m_{\Xi_b} - m_{\Xi})^{B_f}}{\sqrt{(16 + 8 \cdot C_f) \cdot D_f \cdot \pi^2 \cdot \chi_f}} \phi_{f,1}(q^2)^{E_f/4} \phi_{f,2}(q^2)^{F_f/4} \phi_{f,3}(q^2)^{(N_f + G_f)/2} \phi_{f,4}(q^2) \quad (\text{B1})$$

with

$$\phi_{f,1}(q^2) = \frac{s_-(q^2)}{z(q^2, q_{\text{max}}^2, t_+^f)}, \quad (\text{B2})$$

$$\phi_{f,2}(q^2) = s_+(q^2), \quad (\text{B3})$$

$$\phi_{f,3}(q^2) = -\frac{z(q^2, 0, t_+^f)}{q^2}, \quad (\text{B4})$$

$$\phi_{f,4}(q^2) = 2\sqrt{t_+^f - q_{\text{max}}^2} \left[1 + z(q^2, q_{\text{max}}^2, t_+^f)\right]^{1/2} \left[1 - z(q^2, q_{\text{max}}^2, t_+^f)\right]^{-3/2}. \quad (\text{B5})$$

The values of  $N_f$ ,  $\chi_f$ , and  $A_f$  through  $G_f$  are listed in Table XII. Above,  $s_{\pm}(q^2) = (m_{\Xi_b} \pm m_{\Xi})^2 - q^2$ .

$f$	$A_f$	$B_f$	$C_f$	$D_f$	$E_f$	$F_f$	$G_f$	$N_f$	$\chi_f$
$f_0$	0	1	0	1	1	3	3	1	0.0142
$f_+$	1	0	1	2	3	1	3	2	$0.0120/m_b^2$
$f_{\perp}$	0	0	1	1	3	1	2	2	$0.0120/m_b^2$
$g_0$	1	0	1	$\frac{2}{3}$	3	1	3	1	0.0157
$g_+$	0	1	0	3	1	3	3	2	$0.0113/m_b^2$
$g_{\perp}$	0	0	1	1	1	3	2	2	$0.0113/m_b^2$
$h_+$	0	0	1	2	3	1	1	3	$0.00803/m_b^2$
$h_{\perp}$	1	0	1	1	3	1	2	3	$0.00803/m_b^2$
$\tilde{h}_+$	0	0	1	2	1	3	1	3	$0.00748/m_b^2$
$\tilde{h}_{\perp}$	0	1	1	1	1	3	2	3	$0.00748/m_b^2$

TABLE XII. Parameters in the outer functions [117]. Here,  $m_b = 4.2$  GeV.

## Appendix C: Asymptotic-behavior constraints

We define

$$s_0^f = \sum_{n=0}^N a_n^f, \quad (\text{C1})$$

$$s_1^f = \sum_{n=1}^N n a_n^f, \quad (\text{C2})$$

$$s_2^f = \sum_{n=2}^N n(n-1) a_n^f, \quad (\text{C3})$$

$$s_3^f = \sum_{n=3}^N n(n-1)(n-2) a_n^f. \quad (\text{C4})$$

For the form factors  $f_+$ ,  $g_+$ ,  $h_\perp$ , and  $\tilde{h}_\perp$ , we impose the sum rules

$$s_0^f + \sum_{n=N+1}^{N+4} a_n^f = 0, \quad (\text{C5})$$

$$s_1^f + \sum_{n=N+1}^{N+4} n a_n^f = 0, \quad (\text{C6})$$

$$s_2^f + \sum_{n=N+1}^{N+4} n(n-1) a_n^f = 0, \quad (\text{C7})$$

$$s_3^f + \sum_{n=N+1}^{N+4} n(n-1)(n-2) a_n^f = 0, \quad (\text{C8})$$

which we solve for the four coefficients  $a_{N+1}^f, a_{N+2}^f, a_{N+3}^f, a_{N+4}^f$ . Writing

$$j = N + 1, \quad (\text{C9})$$

we obtain

$$a_j^f = -\frac{1}{6}(j+1)(j+2)(j+3)s_0^f + \frac{1}{2}(j+1)(j+2)s_1^f - \frac{1}{2}(j+1)s_2^f + \frac{1}{6}s_3^f, \quad (\text{C10})$$

$$a_{j+1}^f = \frac{1}{2}j(j+2)(j+3)s_0^f - \frac{1}{2}(j+2)(3j+1)s_1^f + \frac{1}{2}(3j+2)s_2^f - \frac{1}{2}s_3^f, \quad (\text{C11})$$

$$a_{j+2}^f = -\frac{1}{2}j(j+1)(j+3)s_0^f + \frac{1}{2}j(3j+5)s_1^f - \frac{1}{2}(3j+1)s_2^f + \frac{1}{2}s_3^f, \quad (\text{C12})$$

$$a_{j+3}^f = \frac{1}{6}j(j+1)(j+2)s_0^f - \frac{1}{2}j(j+1)s_1^f + \frac{j}{2}s_2^f - \frac{1}{6}s_3^f. \quad (\text{C13})$$

For the form factors  $f_0$ ,  $f_\perp$ ,  $g_0$ ,  $g_\perp$ ,  $h_+$ , and  $\tilde{h}_+$ , we impose the sum rules

$$s_0^f + \sum_{n=N+1}^{N+3} a_n^f = 0, \quad (\text{C14})$$

$$s_1^f + \sum_{n=N+1}^{N+3} n a_n^f = 0, \quad (\text{C15})$$

$$s_2^f + \sum_{n=N+1}^{N+3} n(n-1) a_n^f = 0, \quad (\text{C16})$$

which we solve for the three coefficients  $a_{N+1}^f, a_{N+2}^f, a_{N+3}^f$ . Writing again  $j = N + 1$ , the solution in this case is given by

$$a_j^f = -\frac{1}{2}(j+1)(j+2)s_0^f + (j+1)s_1^f - \frac{1}{2}s_2^f, \quad (\text{C17})$$

$$a_{j+1}^f = j(j+2)s_0^f - (2j+1)s_1^f + s_2^f, \quad (\text{C18})$$

$$a_{j+2}^f = -\frac{1}{2}j(j+1)s_0^f + js_1^f - \frac{1}{2}s_2^f. \quad (\text{C19})$$

- 
- [1] B. Capdevila, A. Crivellin, and J. Matias, ‘‘Review of semileptonic B anomalies,’’ *Eur. Phys. J. ST* **1** (2023) 20, [arXiv:2309.01311 \[hep-ph\]](#).  
 [2] **LHCb** Collaboration, R. Aaij *et al.*, ‘‘Measurement of lepton universality parameters in  $B^+ \rightarrow K^+ \ell^+ \ell^-$  and  $B^0 \rightarrow K^{*0} \ell^+ \ell^-$  decays,’’ *Phys. Rev. D* **108** no. 3, (2023) 032002, [arXiv:2212.09153 \[hep-ex\]](#).

- [3] **LHCb** Collaboration, R. Aaij *et al.*, “Test of lepton universality in  $b \rightarrow s\ell^+\ell^-$  decays,” *Phys. Rev. Lett.* **131** no. 5, (2023) 051803, [arXiv:2212.09152 \[hep-ex\]](#).
- [4] S. Descotes-Genon, J. Matias, and J. Virto, “Understanding the  $B \rightarrow K^*\mu^+\mu^-$  Anomaly,” *Phys. Rev. D* **88** (2013) 074002, [arXiv:1307.5683 \[hep-ph\]](#).
- [5] R. R. Horgan, Z. Liu, S. Meinel, and M. Wingate, “Lattice QCD calculation of form factors describing the rare decays  $B \rightarrow K^*\ell^+\ell^-$  and  $B_s \rightarrow \phi\ell^+\ell^-$ ,” *Phys. Rev. D* **89** no. 9, (2014) 094501, [arXiv:1310.3722 \[hep-lat\]](#).
- [6] R. R. Horgan, Z. Liu, S. Meinel, and M. Wingate, “Calculation of  $B^0 \rightarrow K^{*0}\mu^+\mu^-$  and  $B_s^0 \rightarrow \phi\mu^+\mu^-$  observables using form factors from lattice QCD,” *Phys. Rev. Lett.* **112** (2014) 212003, [arXiv:1310.3887 \[hep-ph\]](#).
- [7] W. Altmannshofer and D. M. Straub, “New physics in  $b \rightarrow s$  transitions after LHC run 1,” *Eur. Phys. J. C* **75** no. 8, (2015) 382, [arXiv:1411.3161 \[hep-ph\]](#).
- [8] **LHCb** Collaboration, R. Aaij *et al.*, “Differential branching fractions and isospin asymmetries of  $B \rightarrow K^{(*)}\mu^+\mu^-$  decays,” *JHEP* **06** (2014) 133, [arXiv:1403.8044 \[hep-ex\]](#).
- [9] A. Bharucha, D. M. Straub, and R. Zwicky, “ $B \rightarrow V\ell^+\ell^-$  in the Standard Model from light-cone sum rules,” *JHEP* **08** (2016) 098, [arXiv:1503.05534 \[hep-ph\]](#).
- [10] J. A. Bailey *et al.*, “ $B \rightarrow Kl^+l^-$  Decay Form Factors from Three-Flavor Lattice QCD,” *Phys. Rev. D* **93** no. 2, (2016) 025026, [arXiv:1509.06235 \[hep-lat\]](#).
- [11] R. R. Horgan, Z. Liu, S. Meinel, and M. Wingate, “Rare  $B$  decays using lattice QCD form factors,” *PoS LATTICE2014* (2015) 372, [arXiv:1501.00367 \[hep-lat\]](#).
- [12] **LHCb** Collaboration, R. Aaij *et al.*, “Measurements of the S-wave fraction in  $B^0 \rightarrow K^+\pi^-\mu^+\mu^-$  decays and the  $B^0 \rightarrow K^*(892)^0\mu^+\mu^-$  differential branching fraction,” *JHEP* **11** (2016) 047, [arXiv:1606.04731 \[hep-ex\]](#). [Erratum: *JHEP* 04, 142 (2017)].
- [13] N. Gubernari, A. Kokulu, and D. van Dyk, “ $B \rightarrow P$  and  $B \rightarrow V$  Form Factors from  $B$ -Meson Light-Cone Sum Rules beyond Leading Twist,” *JHEP* **01** (2019) 150, [arXiv:1811.00983 \[hep-ph\]](#).
- [14] **LHCb** Collaboration, R. Aaij *et al.*, “Angular Analysis of the  $B^+ \rightarrow K^{*+}\mu^+\mu^-$  Decay,” *Phys. Rev. Lett.* **126** no. 16, (2021) 161802, [arXiv:2012.13241 \[hep-ex\]](#).
- [15] **LHCb** Collaboration, R. Aaij *et al.*, “Branching Fraction Measurements of the Rare  $B_s^0 \rightarrow \phi\mu^+\mu^-$  and  $B_s^0 \rightarrow f_2'(1525)\mu^+\mu^-$  Decays,” *Phys. Rev. Lett.* **127** no. 15, (2021) 151801, [arXiv:2105.14007 \[hep-ex\]](#).
- [16] N. Gubernari, M. Reboud, D. van Dyk, and J. Virto, “Improved theory predictions and global analysis of exclusive  $b \rightarrow s\mu^+\mu^-$  processes,” *JHEP* **09** (2022) 133, [arXiv:2206.03797 \[hep-ph\]](#).
- [17] **HPQCD** Collaboration, W. G. Parrott, C. Bouchard, and C. T. H. Davies, “ $B \rightarrow K$  and  $D \rightarrow K$  form factors from fully relativistic lattice QCD,” *Phys. Rev. D* **107** no. 1, (2023) 014510, [arXiv:2207.12468 \[hep-lat\]](#).
- [18] **HPQCD** Collaboration, W. G. Parrott, C. Bouchard, and C. T. H. Davies, “Standard Model predictions for  $B \rightarrow K\ell^+\ell^-$ ,  $B \rightarrow K\ell_1^-\ell_2^+$  and  $B \rightarrow K\nu\bar{\nu}$  using form factors from  $N_f = 2 + 1 + 1$  lattice QCD,” *Phys. Rev. D* **107** no. 1, (2023) 014511, [arXiv:2207.13371 \[hep-ph\]](#). [Erratum: *Phys.Rev.D* 107, 119903 (2023)].
- [19] **LHCb** Collaboration, R. Aaij *et al.*, “Determination of short- and long-distance contributions in  $B^0 \rightarrow K^{*0}\mu^+\mu^-$  decays,” *Phys. Rev. D* **109** no. 5, (2024) 052009, [arXiv:2312.09102 \[hep-ex\]](#).
- [20] N. Gubernari, M. Reboud, D. van Dyk, and J. Virto, “Dispersive analysis of  $B \rightarrow K^{(*)}$  and  $B_s \rightarrow \phi$  form factors,” *JHEP* **12** (2023) 153, [arXiv:2305.06301 \[hep-ph\]](#). [Erratum: *JHEP* 01, 125 (2025)].
- [21] **CMS** Collaboration, A. Hayrapetyan *et al.*, “Test of lepton flavor universality in  $B^\pm \rightarrow K^\pm\mu^+\mu^-$  and  $B^\pm \rightarrow K^\pm e^+e^-$  decays in proton-proton collisions at  $\sqrt{s} = 13$  TeV,” *Rept. Prog. Phys.* **87** no. 7, (2024) 077802, [arXiv:2401.07090 \[hep-ex\]](#).
- [22] **CMS** Collaboration, A. Hayrapetyan *et al.*, “Angular analysis of the  $B^0 \rightarrow K^*(892)^0\mu^+\mu^-$  decay in proton-proton collisions at  $\sqrt{s} = 13$  TeV,” *Phys. Lett. B* **864** (2025) 139406, [arXiv:2411.11820 \[hep-ex\]](#).
- [23] **LHCb** Collaboration, R. Aaij *et al.*, “A comprehensive analysis of the  $B^0 \rightarrow K^{*0}\mu^+\mu^-$  decay,” [arXiv:2512.18053 \[hep-ex\]](#).
- [24] **LHCb** Collaboration, R. Aaij *et al.*, “Measurement of the local and nonlocal amplitudes in  $B^+ \rightarrow K^+\mu^+\mu^-$  decays,” [arXiv:2603.12477 \[hep-ex\]](#).
- [25] T. Hurth, F. Mahmoudi, Y. Monceaux, and S. Neshatpour, “Data-driven analyses and model-independent fits for present  $b \rightarrow s\ell\ell$  results,” [arXiv:2508.09986 \[hep-ph\]](#).
- [26] M. Algueró, A. Biswas, B. Capdevila, S. Descotes-Genon, J. Matias, and M. Novoa-Brunet, “To (b)e or not to (b)e: no electrons at LHCb,” *Eur. Phys. J. C* **83** no. 7, (2023) 648, [arXiv:2304.07330 \[hep-ph\]](#).
- [27] T. Hurth, F. Mahmoudi, and S. Neshatpour, “ $B$  anomalies in the post  $R_{K^{(*)}}$  era,” *Phys. Rev. D* **108** no. 11, (2023) 115037, [arXiv:2310.05585 \[hep-ph\]](#).
- [28] Q. Wen and F. Xu, “Global fits of new physics in  $b \rightarrow s$  after the  $R_K^{(*)}$  2022 release,” *Phys. Rev. D* **108** no. 9, (2023) 095038, [arXiv:2305.19038 \[hep-ph\]](#).
- [29] A. Greljo, J. Salko, A. Smolkovič, and P. Stangl, “Rare  $b$  decays meet high-mass Drell-Yan,” *JHEP* **05** (2023) 087, [arXiv:2212.10497 \[hep-ph\]](#).
- [30] A. Khodjamirian, T. Mannel, A. A. Pivovarov, and Y. M. Wang, “Charm-loop effect in  $B \rightarrow K^{(*)}\ell^+\ell^-$  and  $B \rightarrow K^*\gamma$ ,” *JHEP* **09** (2010) 089, [arXiv:1006.4945 \[hep-ph\]](#).
- [31] S. Jäger and J. Martin Camalich, “On  $B \rightarrow V\ell\ell$  at small dilepton invariant mass, power corrections, and new physics,” *JHEP* **05** (2013) 043, [arXiv:1212.2263 \[hep-ph\]](#).
- [32] S. Jäger and J. Martin Camalich, “Reassessing the discovery potential of the  $B \rightarrow K^{(*)}\ell^+\ell^-$  decays in the large-recoil region: SM challenges and BSM opportunities,” *Phys. Rev. D* **93** no. 1, (2016) 014028, [arXiv:1412.3183 \[hep-ph\]](#).

- [33] J. Lyon and R. Zwicky, “Resonances gone topsy turvy - the charm of QCD or new physics in  $b \rightarrow s\ell^+\ell^-$ ?,” [arXiv:1406.0566 \[hep-ph\]](#).
- [34] M. Ciuchini, M. Fedele, E. Franco, S. Mishima, A. Paul, L. Silvestrini, and M. Valli, “ $B \rightarrow K^*\ell^+\ell^-$  decays at large recoil in the Standard Model: a theoretical reappraisal,” *JHEP* **06** (2016) 116, [arXiv:1512.07157 \[hep-ph\]](#).
- [35] C. Bobeth, M. Chrzaszcz, D. van Dyk, and J. Virto, “Long-distance effects in  $B \rightarrow K^*\ell\ell$  from analyticity,” *Eur. Phys. J. C* **78** no. 6, (2018) 451, [arXiv:1707.07305 \[hep-ph\]](#).
- [36] N. Gubernari, D. van Dyk, and J. Virto, “Non-local matrix elements in  $B_{(s)} \rightarrow \{K^{(*)}, \phi\}\ell^+\ell^-$ ,” *JHEP* **02** (2021) 088, [arXiv:2011.09813 \[hep-ph\]](#).
- [37] M. Ciuchini, M. Fedele, E. Franco, A. Paul, L. Silvestrini, and M. Valli, “Constraints on lepton universality violation from rare B decays,” *Phys. Rev. D* **107** no. 5, (2023) 055036, [arXiv:2212.10516 \[hep-ph\]](#).
- [38] T. Feldmann and N. Gubernari, “Non-factorisable contributions of strong-penguin operators in  $\Lambda_b \rightarrow \Lambda\ell^+\ell^-$  decays,” *JHEP* **03** (2024) 152, [arXiv:2312.14146 \[hep-ph\]](#).
- [39] G. Isidori, Z. Polonsky, and A. Tinari, “Explicit estimate of charm rescattering in  $B^0 \rightarrow K^0\bar{\ell}\ell$ ,” *Phys. Rev. D* **111** no. 9, (2025) 093007, [arXiv:2405.17551 \[hep-ph\]](#).
- [40] M. Bordone, G. Isidori, S. Mächler, and A. Tinari, “Short- vs. long-distance physics in  $B \rightarrow K^{(*)}\ell^+\ell^-$ : a data-driven analysis,” *Eur. Phys. J. C* **84** no. 5, (2024) 547, [arXiv:2401.18007 \[hep-ph\]](#).
- [41] T. Hurth, A. Khodjamirian, F. Mahmoudi, D. Mishra, Y. Monceaux, and S. Neshatpour, “Nonlocal form factor of chromomagnetic penguin in  $B \rightarrow K\ell^+\ell^-$  from QCD light-cone sum rules,” [arXiv:2512.10868 \[hep-ph\]](#).
- [42] G. Isidori, Z. Polonsky, and A. Tinari, “Charm rescattering in  $B^0 \rightarrow K^0\bar{\ell}\ell$ : an improved analysis,” *Eur. Phys. J. C* **85** no. 10, (2025) 1221, [arXiv:2507.17824 \[hep-ph\]](#).
- [43] T. Mannel and S. Recksiegel, “Flavor changing neutral current decays of heavy baryons: The Case  $\Lambda_b \rightarrow \Lambda\gamma$ ,” *J. Phys. G* **24** (1998) 979–990, [arXiv:hep-ph/9701399](#).
- [44] G. Hiller and A. Kagan, “Probing for new physics in polarized  $\Lambda_b$  decays at the Z,” *Phys. Rev. D* **65** (2002) 074038, [arXiv:hep-ph/0108074](#).
- [45] P. Böer, T. Feldmann, and D. van Dyk, “Angular Analysis of the Decay  $\Lambda_b \rightarrow \Lambda(\rightarrow N\pi)\ell^+\ell^-$ ,” *JHEP* **01** (2015) 155, [arXiv:1410.2115 \[hep-ph\]](#).
- [46] S. Meinel and D. van Dyk, “Using  $\Lambda_b \rightarrow \Lambda\mu^+\mu^-$  data within a Bayesian analysis of  $|\Delta B| = |\Delta S| = 1$  decays,” *Phys. Rev. D* **94** no. 1, (2016) 013007, [arXiv:1603.02974 \[hep-ph\]](#).
- [47] T. Blake and M. Kreps, “Angular distribution of polarised  $\Lambda_b$  baryons decaying to  $\Lambda\ell^+\ell^-$ ,” *JHEP* **11** (2017) 138, [arXiv:1710.00746 \[hep-ph\]](#).
- [48] D. Das, “Model independent New Physics analysis in  $\Lambda_b \rightarrow \Lambda\mu^+\mu^-$  decay,” *Eur. Phys. J. C* **78** no. 3, (2018) 230, [arXiv:1802.09404 \[hep-ph\]](#).
- [49] H. Yan, “Angular distribution of the rare decay  $\Lambda_b \rightarrow \Lambda(\rightarrow N\pi)\ell^+\ell^-$ ,” [arXiv:1911.11568 \[hep-ph\]](#).
- [50] T. Blake, S. Meinel, and D. van Dyk, “Bayesian Analysis of  $b \rightarrow s\mu^+\mu^-$  Wilson Coefficients using the Full Angular Distribution of  $\Lambda_b \rightarrow \Lambda(\rightarrow p\pi^-)\mu^+\mu^-$  Decays,” *Phys. Rev. D* **101** no. 3, (2020) 035023, [arXiv:1912.05811 \[hep-ph\]](#).
- [51] F. Hussain, J. G. Korner, M. Kramer, and G. Thompson, “On heavy baryon decay form-factors,” *Z. Phys. C* **51** (1991) 321–328.
- [52] F. Hussain, D.-S. Liu, M. Kramer, J. G. Korner, and S. Tawfiq, “General analysis of weak decay form-factors in heavy to heavy and heavy to light baryon transitions,” *Nucl. Phys. B* **370** (1992) 259–277.
- [53] H.-Y. Cheng, C.-Y. Cheung, G.-L. Lin, Y. C. Lin, T.-M. Yan, and H.-L. Yu, “Effective Lagrangian approach to weak radiative decays of heavy hadrons,” *Phys. Rev. D* **51** (1995) 1199–1214, [arXiv:hep-ph/9407303](#).
- [54] H.-Y. Cheng and B. Tseng, “ $1/M$  corrections to baryonic form-factors in the quark model,” *Phys. Rev. D* **53** (1996) 1457, [arXiv:hep-ph/9502391](#). [Erratum: *Phys.Rev.D* 55, 1697 (1997)].
- [55] C.-S. Huang and H.-G. Yan, “Exclusive rare decays of heavy baryons to light baryons:  $\Lambda_b \rightarrow \Lambda\gamma$  and  $\Lambda_b \rightarrow \Lambda\ell^+\ell^-$ ,” *Phys. Rev. D* **59** (1999) 114022, [arXiv:hep-ph/9811303](#). [Erratum: *Phys.Rev.D* 61, 039901 (2000)].
- [56] R. Mohanta, A. K. Giri, M. P. Khanna, M. Ishida, and S. Ishida, “Weak radiative decay  $\Lambda_b \rightarrow \Lambda\gamma$  and quark confined effects in the covariant oscillator quark model,” *Prog. Theor. Phys.* **102** (1999) 645–652, [arXiv:hep-ph/9908291](#).
- [57] X.-G. He, T. Li, X.-Q. Li, and Y.-M. Wang, “PQCD calculation for  $\Lambda_b \rightarrow \Lambda\gamma$  in the standard model,” *Phys. Rev. D* **74** (2006) 034026, [arXiv:hep-ph/0606025](#).
- [58] Y.-m. Wang, Y. Li, and C.-D. Lu, “Rare Decays of  $\Lambda_b \rightarrow \Lambda + \gamma$  and  $\Lambda_b \rightarrow \Lambda + \ell^+\ell^-$  in the Light-cone Sum Rules,” *Eur. Phys. J. C* **59** (2009) 861–882, [arXiv:0804.0648 \[hep-ph\]](#).
- [59] Y.-M. Wang, Y.-L. Shen, and C.-D. Lu, “ $\Lambda_b \rightarrow p, \Lambda$  transition form factors from QCD light-cone sum rules,” *Phys. Rev. D* **80** (2009) 074012, [arXiv:0907.4008 \[hep-ph\]](#).
- [60] T. M. Aliev, K. Azizi, and M. Savci, “Analysis of the  $\Lambda_b \rightarrow \Lambda\ell^+\ell^-$  decay in QCD,” *Phys. Rev. D* **81** (2010) 056006, [arXiv:1001.0227 \[hep-ph\]](#).
- [61] W. Wang, “Factorization of Heavy-to-Light Baryonic Transitions in SCET,” *Phys. Lett. B* **708** (2012) 119–126, [arXiv:1112.0237 \[hep-ph\]](#).
- [62] T. Feldmann and M. W. Y. Yip, “Form factors for  $\Lambda_b \rightarrow \Lambda$  transitions in the soft-collinear effective theory,” *Phys. Rev. D* **85** (2012) 014035, [arXiv:1111.1844 \[hep-ph\]](#). [Erratum: *Phys.Rev.D* 86, 079901 (2012)].
- [63] L. Mott and W. Roberts, “Rare dileptonic decays of  $\Lambda_b$  in a quark model,” *Int. J. Mod. Phys. A* **27** (2012) 1250016, [arXiv:1108.6129 \[nucl-th\]](#).
- [64] T. Mannel and Y.-M. Wang, “Heavy-to-light baryonic form factors at large recoil,” *JHEP* **12** (2011) 067, [arXiv:1111.1849 \[hep-ph\]](#).

- [65] T. Gutsche, M. A. Ivanov, J. G. Korner, V. E. Lyubovitskij, and P. Santorelli, “Rare baryon decays  $\Lambda_b \rightarrow \Lambda l^+ l^-$  ( $l = e, \mu, \tau$ ) and  $\Lambda_b \rightarrow \Lambda \gamma$ : differential and total rates, lepton- and hadron-side forward-backward asymmetries,” *Phys. Rev. D* **87** (2013) 074031, [arXiv:1301.3737 \[hep-ph\]](#).
- [66] Y.-M. Wang and Y.-L. Shen, “Perturbative Corrections to  $\Lambda_b \rightarrow \Lambda$  Form Factors from QCD Light-Cone Sum Rules,” *JHEP* **02** (2016) 179, [arXiv:1511.09036 \[hep-ph\]](#).
- [67] L. Mott and W. Roberts, “Lepton polarization asymmetries for FCNC decays of the  $\Lambda_b$  baryon,” *Int. J. Mod. Phys. A* **30** no. 27, (2015) 1550172, [arXiv:1506.04106 \[nucl-th\]](#).
- [68] R. N. Faustov and V. O. Galkin, “Rare  $\Lambda_b \rightarrow \Lambda \ell^+ \ell^-$  and  $\Lambda_b \rightarrow \Lambda \gamma$  decays in the relativistic quark model,” *Phys. Rev. D* **96** no. 5, (2017) 053006, [arXiv:1705.07741 \[hep-ph\]](#).
- [69] Y. Liu, X. H. Guo, and C. Wang, “Study of two body hadronic decays  $\Lambda_b \rightarrow \Lambda(p)P(V)$  in the instantaneous approximation of the Bethe-Salpeter equation approach,” *Phys. Rev. D* **91** no. 1, (2015) 016006.
- [70] L.-L. Liu, X.-W. Kang, Z.-Y. Wang, and X.-H. Guo, “Rare  $\Lambda_b \rightarrow \Lambda \ell^+ \ell^-$  decay in the Bethe-Salpeter equation approach,” *Chin. Phys. C* **44** no. 8, (2020) 083107, [arXiv:1911.08023 \[hep-ph\]](#).
- [71] L. Yang, J.-J. Han, Q. Chang, and F.-S. Yu, “The  $\Lambda_b \rightarrow \Lambda$  transition form factors in perturbative QCD approach,” *Eur. Phys. J. C* **86** no. 2, (2026) 103, [arXiv:2508.18069 \[hep-ph\]](#).
- [72] L.-S. Lu, C.-D. Lü, Y.-L. Shen, and Y.-B. Wei, “SCET sum rules for  $\Lambda_b \rightarrow \Lambda \ell^+ \ell^-$ ,  $\Lambda \gamma$  decays,” *JHEP* **09** (2025) 172, [arXiv:2506.21419 \[hep-ph\]](#).
- [73] F. Mahmoudi and D. Mishra, “ $\Lambda_b \rightarrow \Lambda$  Form Factors from Light-Cone Sum Rules with  $\Lambda$ -Baryon Distribution Amplitudes,” [arXiv:2601.02302 \[hep-ph\]](#).
- [74] W. Detmold, C. J. D. Lin, S. Meinel, and M. Wingate, “ $\Lambda_b \rightarrow \Lambda \ell^+ \ell^-$  form factors and differential branching fraction from lattice QCD,” *Phys. Rev. D* **87** no. 7, (2013) 074502, [arXiv:1212.4827 \[hep-lat\]](#).
- [75] W. Detmold and S. Meinel, “ $\Lambda_b \rightarrow \Lambda \ell^+ \ell^-$  form factors, differential branching fraction, and angular observables from lattice QCD with relativistic  $b$  quarks,” *Phys. Rev. D* **93** no. 7, (2016) 074501, [arXiv:1602.01399 \[hep-lat\]](#).
- [76] **LHCb** Collaboration, R. Aaij *et al.*, “Measurement of the differential branching fraction of the decay  $\Lambda_b^0 \rightarrow \Lambda \mu^+ \mu^-$ ,” *Phys. Lett. B* **725** (2013) 25–35, [arXiv:1306.2577 \[hep-ex\]](#).
- [77] **LHCb** Collaboration, R. Aaij *et al.*, “Differential branching fraction and angular analysis of  $\Lambda_b^0 \rightarrow \Lambda \mu^+ \mu^-$  decays,” *JHEP* **06** (2015) 115, [arXiv:1503.07138 \[hep-ex\]](#). [Erratum: *JHEP* 09, 145 (2018)].
- [78] **LHCb** Collaboration, R. Aaij *et al.*, “Angular moments of the decay  $\Lambda_b^0 \rightarrow \Lambda \mu^+ \mu^-$  at low hadronic recoil,” *JHEP* **09** (2018) 146, [arXiv:1808.00264 \[hep-ex\]](#).
- [79] S. Meinel, “Status of next-generation  $\Lambda_b \rightarrow p, \Lambda, \Lambda_c$  form-factor calculations,” *PoS LATTICE2023* (2024) 275, [arXiv:2309.01821 \[hep-lat\]](#).
- [80] J. Nicolini, *Study of rare beauty baryon decays with the LHCb detector*. PhD thesis, Tech. U., Dortmund (main), Laboratoire de Physique des 2 Infinis Irène Joliot-Curie, France, Tech. U., Dortmund (main), 5, 2024.
- [81] K. Azizi, Y. Sarac, and H. Sundu, “Light cone QCD sum rules study of the semileptonic heavy  $\Xi_Q$  and  $\Xi'_Q$  transitions to  $\Xi$  and  $\Sigma$  baryons,” *Eur. Phys. J. A* **48** (2012) 2, [arXiv:1107.5925 \[hep-ph\]](#).
- [82] K. Azizi, A. T. Olgun, and Z. Tavukoglu, “Impact of scalar leptoquarks on heavy baryonic decays,” *Adv. High Energy Phys.* **2017** (2017) 7435876, [arXiv:1609.09678 \[hep-ph\]](#).
- [83] P. Nayek, S. Biswas, P. Maji, and S. Sahoo, “Imprints of New Physics in Baryonic Decay  $\Xi_b \rightarrow \Xi \ell^+ \ell^-$  in Non-universal  $Z$  Model,” *Int. J. Theor. Phys.* **59** no. 9, (2020) 2712–2740.
- [84] R.-M. Wang, Y.-G. Xu, C. Hua, and X.-D. Cheng, “Studying  $\mathcal{B}_1(\frac{1}{2}^+) \rightarrow \mathcal{B}_2(\frac{1}{2}^+) \ell^+ \ell^-$  semileptonic weak baryon decays with the SU(3) flavor symmetry,” *Phys. Rev. D* **103** no. 1, (2021) 013007, [arXiv:2101.02421 \[hep-ph\]](#).
- [85] Z. Rui, Z.-T. Zou, Y. Li, and Y. Li, “Semileptonic neutral currents decays of  $\Xi_b$  with dileptons or dineutrinos in the final state,” [arXiv:2512.19429 \[hep-ph\]](#).
- [86] **LHCb** Collaboration, R. Aaij *et al.*, “First Observation of the Radiative Decay  $\Lambda_b^0 \rightarrow \Lambda \gamma$ ,” *Phys. Rev. Lett.* **123** no. 3, (2019) 031801, [arXiv:1904.06697 \[hep-ex\]](#).
- [87] **LHCb** Collaboration, R. Aaij *et al.*, “Search for the radiative  $\Xi_b^- \rightarrow \Xi^- \gamma$  decay,” *JHEP* **01** (2022) 069, [arXiv:2108.07678 \[hep-ex\]](#).
- [88] R.-M. Wang, X.-D. Cheng, Y.-Y. Fan, J.-L. Zhang, and Y.-G. Xu, “Studying radiative baryon decays with the SU(3) flavor symmetry,” *J. Phys. G* **48** no. 8, (2021) 085001, [arXiv:2008.06624 \[hep-ph\]](#).
- [89] A. R. Olamaei and K. Azizi, “Radiative  $\Xi_b^- \rightarrow \Xi^- \gamma$  decay,” *Eur. Phys. J. C* **82** no. 1, (2022) 68, [arXiv:2109.09783 \[hep-ph\]](#).
- [90] C.-Q. Geng, C.-W. Liu, Z.-Y. Wei, and J. Zhang, “Weak radiative decays of antitriplet bottomed baryons in light-front quark model,” *Phys. Rev. D* **105** no. 7, (2022) 073007, [arXiv:2202.06179 \[hep-ph\]](#).
- [91] A. O. Davydov, R. N. Faustov, and V. O. Galkin, “Rare radiative  $\Xi_b^- \rightarrow \Xi^- \gamma$  decay in the relativistic quark model,” *Mod. Phys. Lett. A* **37** no. 24, (2022) 2250158, [arXiv:2208.00833 \[hep-ph\]](#).
- [92] T. M. Aliev, A. Ozpineci, and Y. Sarac, “Reanalysis of rare radiative  $\Xi_b^- \rightarrow \Xi^- \gamma$  decay in QCD,” *Phys. Rev. D* **109** no. 5, (2024) 054020, [arXiv:2312.00461 \[hep-ph\]](#).
- [93] Y.-l. Liu, L.-f. Gan, and M.-q. Huang, “The exclusive rare decay  $b \rightarrow s \gamma$  of heavy b-Baryons,” *Phys. Rev. D* **83** (2011) 054007, [arXiv:1103.0081 \[hep-ph\]](#).
- [94] C. Farrell and S. Meinel, “ $\Xi_c \rightarrow \Xi$  form factors from lattice QCD with domain-wall quarks: A new piece in the puzzle of  $\Xi_c^0$  decay rates,” *Phys. Rev. D* **111** no. 11, (2025) 114521, [arXiv:2504.07302 \[hep-lat\]](#).
- [95] W. Detmold, C. Lehner, and S. Meinel, “ $\Lambda_b \rightarrow p \ell^- \bar{\nu}_\ell$  and  $\Lambda_b \rightarrow \Lambda_c \ell^- \bar{\nu}_\ell$  form factors from lattice QCD with relativistic heavy quarks,” *Phys. Rev. D* **92** no. 3, (2015) 034503, [arXiv:1503.01421 \[hep-lat\]](#).

- [96] S. Meinel, “ $\Lambda_c \rightarrow \Lambda \ell^+ \nu_\ell$  form factors and decay rates from lattice QCD with physical quark masses,” *Phys. Rev. Lett.* **118** no. 8, (2017) 082001, [arXiv:1611.09696 \[hep-lat\]](#).
- [97] S. Meinel, “ $\Lambda_c \rightarrow N$  form factors from lattice QCD and phenomenology of  $\Lambda_c \rightarrow n \ell^+ \nu_\ell$  and  $\Lambda_c \rightarrow p \mu^+ \mu^-$  decays,” *Phys. Rev. D* **97** no. 3, (2018) 034511, [arXiv:1712.05783 \[hep-lat\]](#).
- [98] **RBC, UKQCD** Collaboration, Y. Aoki *et al.*, “Continuum Limit Physics from 2+1 Flavor Domain Wall QCD,” *Phys. Rev. D* **83** (2011) 074508, [arXiv:1011.0892 \[hep-lat\]](#).
- [99] **RBC, UKQCD** Collaboration, T. Blum *et al.*, “Domain wall QCD with physical quark masses,” *Phys. Rev. D* **93** no. 7, (2016) 074505, [arXiv:1411.7017 \[hep-lat\]](#).
- [100] **RBC/UKQCD** Collaboration, Boyle, Peter A. and Del Debbio, Luigi and Garron, Nicolas and Jüttner, Andreas and Soni, Amarjit and Tsang, Justus Tobias and Witzel, Oliver, “SU(3)-breaking ratios for  $D_{(s)}$  and  $B_{(s)}$  mesons,” [arXiv:1812.08791 \[hep-lat\]](#).
- [101] T. Blum, T. Izubuchi, and E. Shintani, “New class of variance-reduction techniques using lattice symmetries,” *Phys. Rev. D* **88** no. 9, (2013) 094503, [arXiv:1208.4349 \[hep-lat\]](#).
- [102] E. Shintani, R. Arthur, T. Blum, T. Izubuchi, C. Jung, and C. Lehner, “Covariant approximation averaging,” *Phys. Rev. D* **91** no. 11, (2015) 114511, [arXiv:1402.0244 \[hep-lat\]](#).
- [103] **RBC, UKQCD** Collaboration, Y. Aoki, N. H. Christ, J. M. Flynn, T. Izubuchi, C. Lehner, M. Li, H. Peng, A. Soni, R. S. Van de Water, and O. Witzel, “Nonperturbative tuning of an improved relativistic heavy-quark action with application to bottom spectroscopy,” *Phys. Rev. D* **86** (2012) 116003, [arXiv:1206.2554 \[hep-lat\]](#).
- [104] Z. S. Brown, W. Detmold, S. Meinel, and K. Orginos, “Charmed bottom baryon spectroscopy from lattice QCD,” *Phys. Rev. D* **90** no. 9, (2014) 094507, [arXiv:1409.0497 \[hep-lat\]](#).
- [105] S. Meinel and G. Rendon, “ $\Lambda_b \rightarrow \Lambda^*(1520) \ell^+ \ell^-$  form factors from lattice QCD,” *Phys. Rev. D* **103** no. 7, (2021) 074505, [arXiv:2009.09313 \[hep-lat\]](#).
- [106] L. Leskovec, S. Meinel, M. Pflaumer, and M. Wagner, “Lattice QCD investigation of a doubly-bottom  $\bar{b}b u d$  tetraquark with quantum numbers  $I(J^P) = 0(1^+)$ ,” *Phys. Rev. D* **100** no. 1, (2019) 014503, [arXiv:1904.04197 \[hep-lat\]](#).
- [107] F. D. R. Bonnet, P. Fitzhenry, D. B. Leinweber, M. R. Stanford, and A. G. Williams, “Calibration of smearing and cooling algorithms in SU(3): Color gauge theory,” *Phys. Rev. D* **62** (2000) 094509, [arXiv:hep-lat/0001018](#).
- [108] C. Morningstar and M. J. Peardon, “Analytic smearing of SU(3) link variables in lattice QCD,” *Phys. Rev. D* **69** (2004) 054501, [arXiv:hep-lat/0311018](#).
- [109] S. Hashimoto, A. X. El-Khadra, A. S. Kronfeld, P. B. Mackenzie, S. M. Ryan, and J. N. Simone, “Lattice QCD calculation of  $\bar{B} \rightarrow D \ell \bar{\nu}$  decay form-factors at zero recoil,” *Phys. Rev. D* **61** (1999) 014502, [arXiv:hep-ph/9906376](#).
- [110] A. X. El-Khadra, A. S. Kronfeld, P. B. Mackenzie, S. M. Ryan, and J. N. Simone, “The Semileptonic decays  $B \rightarrow \pi \ell \nu$  and  $D \rightarrow \pi \ell \nu$  from lattice QCD,” *Phys. Rev. D* **64** (2001) 014502, [arXiv:hep-ph/0101023](#).
- [111] M. Marshall, *Lattice determination of semi-leptonic, heavy-light meson decay form factors*. PhD thesis, Edinburgh U., Edinburgh U., 2024.
- [112] C. Lehner, “Automated lattice perturbation theory and relativistic heavy quarks in the Columbia formulation,” PoS **LATTICE2012** (2012) 126, [arXiv:1211.4013 \[hep-lat\]](#).
- [113] **RBC/UKQCD** Collaboration, J. M. Flynn, R. C. Hill, A. Jüttner, A. Soni, J. T. Tsang, and O. Witzel, “Exclusive semileptonic  $B_s \rightarrow K \ell \nu$  decays on the lattice,” *Phys. Rev. D* **107** no. 11, (2023) 114512, [arXiv:2303.11280 \[hep-lat\]](#).
- [114] W. I. Jay and E. T. Neil, “Bayesian model averaging for analysis of lattice field theory results,” *Phys. Rev. D* **103** (2021) 114502, [arXiv:2008.01069 \[stat.ME\]](#).
- [115] E. T. Neil and J. W. Sitison, “Model averaging approaches to data subset selection,” *Phys. Rev. E* **108** no. 4, (2023) 045308, [arXiv:2305.19417 \[stat.ME\]](#).
- [116] C. G. Boyd, B. Grinstein, and R. F. Lebed, “Constraints on form-factors for exclusive semileptonic heavy to light meson decays,” *Phys. Rev. Lett.* **74** (1995) 4603–4606, [arXiv:hep-ph/9412324](#).
- [117] T. Blake, S. Meinel, M. Rahimi, and D. van Dyk, “Dispersive bounds for local form factors in  $\Lambda_b \rightarrow \Lambda$  transitions,” *Phys. Rev. D* **108** no. 9, (2023) 094509, [arXiv:2205.06041 \[hep-ph\]](#).
- [118] J. M. Flynn, A. Jüttner, and J. T. Tsang, “Bayesian inference for form-factor fits regulated by unitarity and analyticity,” *JHEP* **12** (2023) 175, [arXiv:2303.11285 \[hep-ph\]](#).
- [119] **Particle Data Group** Collaboration, S. Navas *et al.*, “Review of particle physics,” *Phys. Rev. D* **110** no. 3, (2024) 030001.
- [120] C. Bourrely, I. Caprini, and L. Lellouch, “Model-independent description of  $B \rightarrow \pi \ell \nu$  decays and a determination of  $|V_{ub}|$ ,” *Phys. Rev. D* **79** (2009) 013008, [arXiv:0807.2722 \[hep-ph\]](#). [Erratum: *Phys.Rev.D* 82, 099902 (2010)].
- [121] W. W. Buck and R. F. Lebed, “New constraints on dispersive form-factor parameterizations from the timelike region,” *Phys. Rev. D* **58** (1998) 056001, [arXiv:hep-ph/9802369](#).
- [122] T. Becher and R. J. Hill, “Comment on form-factor shape and extraction of  $|V_{ub}|$  from  $B \rightarrow \pi \ell \nu$ ,” *Phys. Lett. B* **633** (2006) 61–69, [arXiv:hep-ph/0509090](#).
- [123] A. Khodjamirian, C. Klein, T. Mannel, and Y. M. Wang, “Form Factors and Strong Couplings of Heavy Baryons from QCD Light-Cone Sum Rules,” *JHEP* **09** (2011) 106, [arXiv:1108.2971 \[hep-ph\]](#).
- [124] J.-L. Zhou and Y.-K. Huang, “Next-to-Leading Order QCD Corrections to  $\Lambda_b \rightarrow p$  Form Factors from Light-Cone Sum Rules,” [arXiv:2602.18050 \[hep-ph\]](#).
- [125] Please see the Supplemental Material for files containing the accepted samples of the form-factor parameters, their mean and covariance matrix, as well as the central values and covariance matrix from the initial fit prior to the “reweighting” procedure.
- [126] D. Du, A. X. El-Khadra, S. Gottlieb, A. S. Kronfeld, J. Laiho, E. Lunghi, R. S. Van de Water, and R. Zhou,

- “Phenomenology of semileptonic B-meson decays with form factors from lattice QCD,” *Phys. Rev. D* **93** no. 3, (2016) 034005, [arXiv:1510.02349 \[hep-ph\]](#).
- [127] M. Beneke, T. Feldmann, and D. Seidel, “Systematic approach to exclusive  $B \rightarrow Vl^+l^-$ ,  $V\gamma$  decays,” *Nucl. Phys. B* **612** (2001) 25–58, [arXiv:hep-ph/0106067](#).
- [128] H. H. Asatryan, H. M. Asatrian, C. Greub, and M. Walker, “Calculation of two loop virtual corrections to  $b \rightarrow sl^+l^-$  in the standard model,” *Phys. Rev. D* **65** (2002) 074004, [arXiv:hep-ph/0109140](#).
- [129] B. Grinstein and D. Pirjol, “Exclusive rare  $B \rightarrow K^*\ell^+\ell^-$  decays at low recoil: Controlling the long-distance effects,” *Phys. Rev. D* **70** (2004) 114005, [arXiv:hep-ph/0404250](#).
- [130] C. Greub, V. Pilipp, and C. Schubach, “Analytic calculation of two-loop QCD corrections to  $b \rightarrow sl^+l^-$  in the high  $q^2$  region,” *JHEP* **12** (2008) 040, [arXiv:0810.4077 \[hep-ph\]](#).
- [131] M. Beylich, G. Buchalla, and T. Feldmann, “Theory of  $B \rightarrow K^{(*)}\ell^+\ell^-$  decays at high  $q^2$ : OPE and quark-hadron duality,” *Eur. Phys. J. C* **71** (2011) 1635, [arXiv:1101.5118 \[hep-ph\]](#).
- [132] **EOS Authors** Collaboration, D. van Dyk *et al.*, “EOS: a software for flavor physics phenomenology,” *Eur. Phys. J. C* **82** no. 6, (2022) 569, [arXiv:2111.15428 \[hep-ph\]](#).
- [133] **UTfit** Collaboration. <http://utfit.org/UTfit/ResultsSummer2025SM>.
- [134] J. Towns, T. Cockerill, M. Dahan, I. Foster, K. Gaither, A. Grimshaw, V. Hazlewood, S. Lathrop, D. Lifka, G. D. Peterson, R. Roskies, J. R. Scott, and N. Wilkins-Diehr, “XSEDE: Accelerating Scientific Discovery,” *Computing in Science Engineering* **16** no. 5, (2014) 62–74.
- [135] T. J. Boerner, S. Deems, T. R. Furlani, S. L. Knuth, and J. Towns, “ACCESS: Advancing Innovation: NSF’s Advanced Cyberinfrastructure Coordination Ecosystem: Services & Support,” in *Practice and Experience in Advanced Research Computing 2023: Computing for the Common Good*, PEARC ’23, p. 173–176. Association for Computing Machinery, New York, NY, USA, 2023. <https://doi.org/10.1145/3569951.3597559>.
- [136] **SciDAC**, **LHPC**, **UKQCD** Collaboration, R. G. Edwards and B. Joo, “The Chroma software system for lattice QCD,” *Nucl. Phys. B Proc. Suppl.* **140** (2005) 832, [arXiv:hep-lat/0409003](#).
- [137] R. G. Edwards, B. Joó, *et al.*, “Chroma.” <https://github.com/JeffersonLab/chroma>.
- [138] A. Pochinsky, S. Syritsyn, *et al.*, “QLUA.” <https://usqcd.lns.mit.edu/w/index.php/QLUA>.
- [139] A. Pochinsky, S. Syritsyn, *et al.*, “Möbius Domain Wall inverter.” <https://github.com/usqcd-software/mdwf>.
- [140] **USQCD** Collaboration, “USQCD Software.” <http://usqcd-software.github.io>.
- [141] C. G. Boyd and M. J. Savage, “Analyticity, shapes of semileptonic form-factors, and  $\bar{B} \rightarrow \pi\ell\bar{\nu}$ ,” *Phys. Rev. D* **56** (1997) 303–311, [arXiv:hep-ph/9702300](#).
- [142] I. Caprini, *Functional Analysis and Optimization Methods in Hadron Physics*. Springer Briefs in Physics. Springer, 2019.